Exploring Novel Aluminum Chemistry Using Quantum Mechanical Computations

by

Katherine Rose Compaan

(Under the Direction of Henry F. Schaefer III)

Abstract

Quantum mechanical computational methods are applied to a variety of aluminum-containing molecules. A novel recently-synthesized organoaluminum compound, bis-pentamethylcyclopentadienyl diiododialane ($Cp^*_2Al_2I_2$), was investigated using density functional and *ab initio* methods. A family of twenty related compounds was constructed to systematically investigate halogen and ligand effects. Electronic effects are most important in species with small alkyl ligands (H or methyl), while steric repulsions dominate in species with bulky ligands (cyclopentadienyl or pentamethylcyclopentadienyl). These effects were discussed in detail using natural bond orbital analysis. Next, the small molecules $AlCH_2$ and $AlCH_2^+$ were investigated using highly accurate *ab initio* methods. There is an Al–C single bond in the neutral, but the AlC interaction in the cation is a half-bond. Both are thermodynamically stable with respect to dissociation, and may be observable in the interstellar medium. Highly accurate spectroscopic constants were computed to aid astrochemists in identifying these species.

Index words: Computational Chemistry, Theoretical Chemistry, Inorganic Chemistry, Aluminum Chemistry, Sandwich Compounds, Astrochemistry

Exploring Novel Aluminum Chemistry Using Quantum Mechanical Computations

by

Katherine Rose Compaan

B.S., University of North Florida, 2008

A Dissertation Submitted to the Graduate Faculty
of The University of Georgia in Partial Fulfillment
of the
Requirements for the Degree

Doctor of Philosophy

Athens, Georgia

2012

Exploring Novel Aluminum Chemistry Using Quantum Mechanical Computations

by

Katherine Rose Compaan

Major Professor: Henry F. Schaefer III

Committee: Nigel G. Adams
Geoffrey D. Smith

Electronic Version Approved:

Maureen Grasso
Dean of the Graduate School
The University of Georgia
May 2012

ACKNOWLEDGEMENTS

First, I must acknowledge my parents, Anthony and Carol Compaan, for providing a loving and supportive home throughout my childhood and education. They have always been prayerful and encouraging, especially during this new endeavor of graduate school. I am grateful to Dr. Robert Vergenz, who taught me undergraduate level physical chemistry and introduced me to quantum chemistry during my junior year of college. Under his guidance, I was able to complete my first research project, attend my first scientific conference, and publish my first paper. It was entirely due to his persistent reminders that I visited UGA and met my graduate advisor, Professor Henry F. Schaefer III.

Professor Schaefer has been a pleasure to work for during the past four years. I desire to emulate his dedication to high quality scientific research. His gracious and friendly attitude toward students is admirable. He provides his students with a building and work atmosphere that encourage productive collaboration, mentoring relationships, and learning. I am also grateful for the generous Robert S. Mulliken research fellowship he provided for me. Mrs. Linda Rowe and Mrs. Amy Peterson have been invaluable in navigating through the paperwork associated with acquiring a graduate degree and have become friends.

I must thank my dear friends and colleagues, Dr. Qianyi Cheng and (soon to be Dr.) Beulah Narendrapurapu. They have become close personal friends, as well as lending sympathetic ears, and often useful suggestions, during research difficulties at the CCQC. Thanks to Dr. Justin Turney and Dr. Andrew Simmonett for providing valuable guidance through research projects and technical difficulties. My friends, Brandon Magers, Peter Ascik, David

Hollman, Alex Vaughn, and Kedan He, along with Beulah, made up one of the most fruitful study groups I have ever known. Working on quantum chemistry homework sets in the wee hours of the morning with you all will be a fond memory of graduate school. The University of Georgia faculty members, Professor Allen, Doctor Yamaguchi, Professor Schleyer, Professor Duncan, and Professor Robinson taught extremely valuable classes and provided helpful discussions on multiple occasions during my studies. Finally, I must thank my church and Georgia Christian Grads, for providing much-needed reminders of my real priorities.

CONTENTS

CHAPTER 1

INTRODUCTION AND LITERATURE REVIEW

1.1 Aluminum Chemistry

Aluminum is the most abundant metal on earth, comprising 8% of the earth's crust[1], but our understanding of aluminum chemistry is still somewhat limited. The chemistry of aluminum (II)[2], in which the aluminum atom bears a formal +2 charge, is particularly underdeveloped, while more is known about monovalent and trivalent aluminum[3,4]. It is a newly burgeoning field of chemical research, since laboratories have only recently become capable of handling air-sensitive low-valent aluminum compounds[2,3]. Furthermore, aluminum (I) compounds are precursors to exotic bicyclo and spiro species[4], and low-valent aluminum species may play important roles in radical and photoinduced reactions[2]. In my research, I am furthering our understanding of Al(0), Al (I) and Al(II) compounds by computationally studying molecules which are not currently accessible to experimental studies.

1.2 Quantum Chemistry

Computational quantum chemistry endeavors to understand the structures, properties, and reactivities of molecules by solving the time independent electronic Schrödinger equation[5].

$$\hat{H}\Psi = E\Psi \ . \tag{1.1}$$

In this equation, Ψ is the wavefunction: a mathematical description of the molecular system which depends on the spatial and spin coordinates of all the particles (nuclei and electrons). The Hamiltonian, $\hat{H}$, is the energy operator; it describes all of the kinetic (T) and potential (V) energies related to the system. E is the absolute energy of the system. The Hamiltonian can be broken down into several individual contributions.

$$\hat{H} = \hat{T}_{nuc} + \hat{T}_{elec} + \hat{V}_{nuc-nuc} + \hat{V}_{nuc-elec} + \hat{V}_{elec-elec} \tag{1.2}$$

The first two terms are kinetic energy terms; term, $\hat{T}_{nuc}$, describes the kinetic energy of the nuclei and $\hat{T}_{elec}$ is the kinetic energy of the electrons. The third term accounts for nuclear-nuclear repulsion. The fourth term, $\hat{V}_{nuc-elec}$, is nuclear-electronic attraction, and the final term, $\hat{V}_{elec-elec}$, deals with electron-electron repulsion. Under the Born-Oppenheimer approximation (BOA)[6], the large disparity between nuclear and electronic masses is used to make a sudden-adiabatic approximation. The nuclei are considered to be clamped in place while the much lighter electrons move around the nuclear framework. Since the nuclei are either stationary or moving at a constant velocity through space, $\hat{T}_{nuc}$ is either zero or constant. Only relative energies are relevant and thus $\hat{T}_{nuc}$ may be ignored. In addition, under the BOA, the $\hat{V}_{nuc-nuc}$ term becomes a constant, easily computed using Coulomb's law. The number of variables is greatly reduced in the Born-Oppenheimer approximation, since the nuclear coordinates are constant parameters. Accurate molecular geometries can be computed by finding the arrangement of nuclei that yields the lowest total energy in a process called geometry optimization. After applying the BOA, we are left with a simplified Schrödinger equation, consisting of an electronic Hamiltonian ($\hat{H}_{elec}$) and a constant nuclear-nuclear repulsion term ($\hat{V}_{nuc-nuc}$), with the Born-Oppenheimer energy as the eigenvalue (E_{BOA}).

$$\hat{H}_{elec} = \hat{T}_{elec} + \hat{V}_{nuc-elec} + \hat{V}_{elec-elec} \tag{1.3}$$

$$(\hat{H}_{el} + \hat{V}_{nuc-nuc})\Psi_{elec} = E_{BOA}\Psi_{elec} \tag{1.4}$$

This differential eigenvalue problem is rather simple to solve for one-electron systems, using normal analytical methods for differential equations. However, it becomes impossible to solve analytically for systems with multiple electrons using current techniques. Because of this difficulty, there are a few different approaches to computing the energy of a many-electron system. Two approaches are used in this dissertation. The first approach uses post Hartree Fock *ab initio* methods. *Ab initio* methods rely only on the physics of the system to determine the appropriate Hamiltonian, and do not incorporate any experimental parameters. The second approach is density functional theory (DFT), which employs approximate mathematical forms based on experimental data.

1.2.1 Hartree-Fock Theory

The Hartree Fock (HF) approximation solves the Schrödinger equation for a many-electron system by assuming that the molecular wavefunction can be written as a single linear combination of atomic wavefunctions. In the words of Professor Schaefer, "The Hartree-Fock wavefunction is the best possible, in the variational sense, single-determinant wavefunction." The atomic wavefunctions resemble the electronic orbitals of hydrogenic systems, like those encountered in an undergraduate physical chemistry course. Neglecting the details of writing this wavefunction as a determinant in order to obey antisymmetry rules, the HF wavefunction is the set of molecular orbitals (MOs), occupied according to the Aufbau principle, which gives the lowest value of E_{elec}. Since the wavefunction is composed of a single determinant of one-electron basis functions, the $\hat{V}_{elec-elec}$ term is not exact. Each electron "feels"

the potential generated by all of the other electrons, but it does not avoid every other electron individually. The difference between the HF energy and the true energy is called the correlation energy. It arises from neglect of instantaneous interelectron interactions.

The HF method accounts for the majority of the electronic energy of a molecule, but in order to get relative energies with chemical accuracy (within 1 kcal mol^{-1}), we must go beyond the HF approximation. However, most *ab initio* methods are based on HF reference wavefunctions, so HF is an essential first step. In addition, the HF method is rigorously variational; it provides an upper-bound to the true energy.

1.2.2 Post-Hartree-Fock Methods

In order to get the true electronic energy of a molecule, computations must "recover" the correlation energy. The traditional approach for recovering correlation energy is called full configuration interaction (FCI). This method expands the HF wavefunction to include "excited" determinants; electron distributions in which an electron has been promoted from an occupied HF MO into a higher-energy unoccupied orbital. The FCI wavefunction consists of a linear combination of the HF determinant with all possible excited determinants. This method accounts for correlation by allowing the electrons to instantaneously avoid each other by moving into higher-energy orbitals. With an infinite basis set, FCI gives the exact electronic energy within the limits of the BOA. However, the number of excited determinants increases factorially with increasing basis set size. Thus, FCI is only applicable to systems with small numbers of electrons. Truncated CI methods, in which only single excitations (CIS) or only single and double excitations (CISD), are cheaper but suffer from improper dissociation behavior. They are not useful for computing reaction energies.

The simplest method for recovering some of the correlation energy is second order Møller-Plessett perturbation theory (MP2). In this approach, the exact energy operator (Hamil-

tonian) is split into a HF term and a perturbation term. After working through the linear algebra, the MP2 energy is given by the following equation.[7]

$$E_{MP2} = E_{HF} + \sum_{i<j}^{occ} \sum_{a<b}^{vir} \frac{(\langle \phi_i \phi_j | \phi_a \phi_b \rangle - \langle \phi_i \phi_j | \phi_b \phi_a \rangle)}{\epsilon_i + \epsilon_j - \epsilon_a - \epsilon_b} \tag{1.5}$$

Molecular orbitals are denoted ϕ. The "occ" and "vir" spaces refer to occupied HF MOs and unoccupied HF MOs, respectively. The shorthand for integrals is as follows, where 1 and 2 refer to all spatial and spin coordinates of two electrons, and r_{12} is the distance between the two electrons.

$$\langle \phi_p \phi_q | \phi_r \phi_s \rangle \equiv \int \frac{\phi_p(1)\phi_q(1)\phi_r(2)\phi_s(2)}{r_{12}} d\tau \tag{1.6}$$

Thus, one only needs the HF wavefunction and some additional integrals based on HF MOs to compute the MP2 energy. Despite its low computational cost, MP2 performs very well in most cases. However, it is not a variational method. That is, the MP2 energy may be lower or higher than the actual energy of the system.

Coupled cluster (CC) methods use an exponential "excitation operator" which acts on a HF reference wavefunction to build in electron correlation[7].

$$\psi_{CC} = e^T \psi_{HF} \tag{1.7}$$

$$e^T = 1 + T + \frac{1}{2}T^2 + \frac{1}{6}T^3 ... \tag{1.8}$$

Coupled cluster methods are mathematically and computationally more tractable than FCI, and exhibit proper dissociation behaviour. The full expansion from Equation 1.8 yields the exact electronic energy, if used in conjunction with an infinite basis set. More commonly, truncated CC methods are employed. CCSD incorporates single and double electron exci-

tations[8–10], while CCSD(T)[11] is the CCSD energy with a perturbative correction for triple excitations. Incorporation of full triple excitations is denoted CCSDT, while CCSDTQ has everything up to quadruple excitations. Currently, the "gold standard" computational method for geometry optimization is CCSD(T) with a moderately large basis set such as cc-pVTZ or cc-pVQZ. This method is is computationally feasible for many small systems on research-grade computer clusters, and the results are generally highly accurate. CCSD(T) cc-pVQZ bond lengths are expected to be accurate to 0.01Å, and bond angles to 1°.

1.2.3 Focal Point Analysis

In order to determine reaction energies or relative energies more accurately than cc-pVQZ CCSD(T), computational chemists often use the focal point approach (FPA) developed by Allen and coworkers[12–18]. FPA assumes that geometries determined at lower levels of theory are sufficiently accurate, and that the inaccuracy in relative energies is mainly due to insufficient treatment of electron correlation. Geometry optimizations are significantly more expensive computationally than an energy computation at a fixed geometry. Thus, after computing the geometry at the highest level of theory feasible, single-point energy computations are performed at several higher levels of theory.

In well-behaved systems, the difference between HF and MP2 energies is much larger than the difference between MP2 and CCSD. The difference between CCSD and CCSD(T) will be much smaller than either of these. In other words, successively higher excitations become systematically less important. Increasing the basis set size provides more flexibility for the wavefunction and increases the accuracy of the energy at each (variational) level of theory. However, at some finite basis set size, the system will have sufficient basis functions to describe the system. Increasing the basis set further will not change the energy. Based on these two trends, the focal point approach of Allen uses multiple computations to monitor the convergence of the system's energy to the FCI CBS (complete basis set) limit[12–18]. The

Table 1.1: Focal point analysis of the torsional barrier for Al_2H_4 in kcal mol^{-1}. Energies were computed at DZP B3LYP geometries.

	ΔE_{HF}	$+\delta$[MP2]	$+\delta$[CCSD]	$+\delta$[CCSD(T)]	$\Delta E_{CCSD(T)}$
aug-cc-pVDZ	+0.81	+0.21	−0.05	+0.05	[+1.02]
aug-cc-pVTZ	+0.88	+0.23	−0.08	+0.06	[+1.09]
aug-cc-pVQZ	+0.84	+0.21	−0.07	+0.07	[+1.04]
CBS LIMIT	[+0.84]	[+0.19]	[−0.07]	[+0.07]	[+**1.03**]
Fit	$a + (X+1)be^{-9\sqrt{X}}$	$a + bX^{-3}$	$a + bX^{-3}$	$a + bX^{-3}$	

most intuitive way to present this information is in an incremented focal point table, an example of which is shown above[19].

The rows cooresponds to basis sets, and columns correspond to levels of theory. The entries in the first column are the HF estimates of the rotational barrier, and subsequent columns contain incremented corrections to the HF estimate. An appropriate mathematical form is used to extrapolate each column to the CBS limit; the formulae are shown in the last row for completeness. While the values in the MP2 column are relatively large, the CCSD and CCSD(T) corrections are quite small. The best estimate of the rotational barrier is the bottom right entry in the table, 1.03 kcal mol^{-1}. This is an estimate of the CCSD(T) rotational barrier at the CBS limit. Note that this estimate is based on geometries computed with a very inexpensive computational method, DFT (see next section). In addition, this focal point table shows that the rotational barrier is nearly converged with respect to basis set; the difference between aug-cc-pVTZ and aug-cc-pVQZ energies is less than 0.02 kcal mol^{-1} using any method.

The FPA is very flexible because the table can always be extended if the convergence is not satisfactory. For instance, larger basis sets (more rows) or more extensive correlation treatments (more columns) can be added to reach the desired convergence for a given project.

FPA also allows chemists to determine the uncertainty associated with the FP estimate of a relative energy. For instance, in the table shown above, the torsional barrier is accurate to within 0.05 kcal mol^{-1}. Finally, FPA serves as a diagnostic for well-behaved systems. Well-behaved systems converge relatively smoothly to the CBS FCI limit. If higher level corrections increase in magnitude across the focal point table, the system is not described well by a single-reference wavefunction, and multireference methods must be employed. Multireference methods are designed for molecules in which the ground state wavefunction cannot be described by a single HF reference. The ground state wavefunction has significant ($> 10\%$) contributions from other HF reference wavefunctions. However, multireference methods were not necessary to complete this dissertation.

1.2.4 Density Functional Theory

DFT is a radically different way of determining the electronic energy[20]. It is, in principle, exact. Given the electron density (ρ), it can be shown that there is a functional ($\hat{F}$) which operates on the density and returns the energy (E). A given electron density corresponds to a unique energy of the system.

$$\hat{F}\,\rho(x,y,z) = E \tag{1.9}$$

The advantage of DFT is that the electron density is a function of only three variables (x,y,z), instead of three coordinates for each electron. For large systems, this very greatly reduces the number of variables. Thus, DFT is applicable to systems too large to handle with current *ab initio* methods. The difficulty with DFT is that $\hat{F}$ remains a mystery; both the mathematical form and the route to determining $\hat{F}$ are unknown. Approximate functionals have been constructed by fitting to empirical or reliable *ab initio* data. A very popular DFT method, B3LYP, has three parameters based on experimental data[21,22]. It gives generally

satisfactory results and is quite computationally inexpensive. DFT is especially useful when benchmarked against high quality *ab initio* results on model systems, in order to determine the accuracy of the functional for that application. There are many functionals available in common quantum chemistry packages[23]. Depending on the data used to parameterize the functional, it may perform well on certain types of molecules (e.g. organic species) but poorly on other types (e.g. metal complexes). DFT methods must be chosen with care, and the results must be interpreted cautiously.

1.3 $Cp^*_2Al_2I_2$ And Its Derivatives

In the first chapter, I investigated a recently-synthesized sandwich compound, bis-pentamethylcyclopentadienyl diiododialane ($Cp^*_2Al_2I_2$)[24]. This molecule was of interest because homonuclear-bonding between group 13 elements is relatively rare[25–27]. Some of the known Al−Albonds are between aluminum (II) atoms,[28–32] but none of them involve cyclopentadienyl (Cp) type ligands. In addition, $Cp^*_2Al_2I_2$ is an intermediate in the modern synthesis of Cp^*Al_4[33], which is a cornerstone of organoaluminum chemistry. It is a precursor to aluminum-transition-metal bonds[34–37] aluminum-boron donor-acceptor bonds[38], aluminum clusters[39], and iminoalanes[40,41]. Aluminum clusters are of interest because they represent an intermediate case between molecular and metallic Al−Al bonding[39,42–50].

The first dialane, or non-metallic Al−Al bond, was reported in 1988[51]. The Al−Al bond was supported by bis(trimethylsilyl)methyl ligands; such bulky ligands prevent the aluminum core from polymerizing[52] or disproportionating to aluminum metal[53]. The Al−Al distances in dialanes range from 2.5 to 2.9 Å, which is somewhat shorter than the metallic Al−Al distance of 2.86Å[1]. There are even instances of one-electron π-bonds in dialanes[28,54–59]. An additional electron resides along the Al−Al bond, resulting in a radical anion with an Al-Al distance shorter than the parent compound. There have also been reports of true Al−Al double bonds[30,31], but such compounds proved troublesome to isolate and characterize.

$Cp^*_4Al_4$ was the first aluminum (I) compound found to be stable at room temperature[60]. It consists of a tetrahedral core of aluminum atoms, surrounded by four η^5 coordinated pentamethylcyclopentadienyl (Cp^*) rings[60]. This aesthetically pleasing molecule was synthesized just three years after the first dialane. A large variety of ligands can support a tetrahedral Al_4 core. Several Cp derivatives have been used[53,61], as well as tBu$_3$SiAl[62,63], C(SiMe$_3$)$_3$[64], Si(SiMe$_3$)$_3$[65], and 2,6-iPr$_2$C$_6$H$_3$N(SiMe$_3$)[66]. Even the simplest ligands, hydrogen atoms, can support a nearly-tetrahedral Al_4 core in the gas phase[67]; there are also substituted versions of the Al_4H_6 cluster[68]. Werner Uhl reviewed tetrahedral aluminum clusters, noting in particular their "aesthetic charm" and "unique bonding situation"[69]. Highly delocalized molecular orbitals facilitate the metal-metal bonding[69]. All Cp-type ligands bond to the core through π-type bonds, while other ligands form σ-type bonds[4]. However, physical property disparities between Cp_4Al_4 and $Cp^*_4Al_4$ are not well understood. For instance, $Cp^*_4Al_4$ does not degrade at temperatures up to 140°C, while Cp_4Al_4 disproportionates at any temperature above -50°C[53]. The intermediate to disproportionation is an $Al_{50}Cp_{12}$ cluster, which has a metallic core[49]. The intermediate forms easily if the Cp rings are not methylated, but there is a large barrier to its formation with methylated Cp rings[70]. Although this phenomenon has been identified, it is still not understood[70].

Despite the importance of organoaluminum chemistry, there have been very few computational studies on Al−Al bonded organometallics. Early computational work focused on the bonding[62,71] and ^{27}Al NMR shifts[72] of AlR tetramers, where R is a halide or alkyl ligand. A few experimental results on organoaluminum compounds have been interpreted with the aid of DFT computations[32,53,63,73]. Very small organoaluminum compounds, such as Al_2H_4 have been studied more extensively. The global minimum on the Al_2X_4 (X=H,F,Cl) potential energy surface[73,74] is $AlX_4^-Al^+$, but $H_2Al{-}AlH_2$ is of interest as the aluminum analog of ethylene and because it has been isolated in matrix experiments[75,76]. Suitable electron-donating groups can stabilize the $X_2Al{-}AlX_2$ geometry[3]. For these reasons, the

global potential energy surface has been explored[74,77,78] and molecular orbitals have been computed[79]. Interestingly, $X_2Al{-}AlX_2$ (X=H, F, Cl, Br, I) prefers a twisted (D_{2d}) geometry to a planar (D_{2h}) geometry[80]. Furthermore, in that series, the hydrogen derivative has by far the largest barrier to rotation about the Al−Al bond[80]. This is due to a tension between electronic and steric effects, further explored in my research.

1.4 $AlCH_2$, $AlCH_2^+$ And Their Structural Isomers

In the next project, I worked on the small molecules $AlCH_2$, HAlCH, $AlCH_2^+$, and $HAlCH^+$. These projects were motivated by an interest in identifying new molecules in the interstellar medium (ISM). A handful of aluminum-bearing molecules have been detected in the ISM[81–86], as well as the CH_2 molecule, methylene[87]. Understanding which molecules are present in the ISM and in what quantities will lead to improved models of the complex chemistry that takes place around hot cores. These are the regions of the ISM in which hydrogen and helium undergo fusion to form heavier nuclei[88,89]. Since the rotational bands of methylene are obscured by other species in the ISM[87], detection of $AlCH_2$ could be an indirect means of quantifying interstellar methylene.

The rich microwave spectra obtained from telescopic observations contain detailed rotational spectra of species present in the ISM. Decrypting these spectra in order to identify specific molecular contributors is an enormous task, and requires data from terrestrial experiments or computations. For instance, the identification of AlNC in the cloud IRC + 10216 relied heavily on both computational[90,91] and experimental data[91–96] to definitively confirm the existence of AlNC in the ISM[81,89,97].

$AlCH_2$ has been the subject of a few low-level computational studies. The first, which simply computed HF geometries, was published in 1980[98]. Subsequent work refined the geometries[99–101]. The highest level of theory employed in previous studies was CISD with a TZ2P basis set[100,101]. Properties were computed using UMP2 with a Pople basis set

(6-311G**)[102]. With improved computational facilities, a highly accurate investigation of $AlCH_2$ and $AlCH_2^+$ seemed in order.

$AlCH_2$ has been detected experimentally[103–105] in gas-phase mass spectrometry experiments. However, its rotational and vibrational spectra have not been recorded, nor is there any work on $AlCH_2^+$ to our knowledge. The full potential energy surface of $AlCH_2$ and its cation are also of interest, since experiments did not detect HAlCH isomers after fragmentation of trimethylaluminum[103]. However, the HAlCH isomer may exist in the gas phase, if it is protected by sufficiently high potential energy barriers. Chemistry in the ISM is primarily kinetically controlled, due to the low densities and temperatures[88]. Structures which represent local minima on the potential energy surface may be frozen in that configuration, since they do not have sufficient energy to escape.

Finally, studies on small molecules like $AlCH_2$ highlight the drastic differences between carbon chemistry and the behavior of other elements. For instance, on the C_2H_2 potential energy surface, the linear acetylene (HCCH) is the global minimum[106,107], while the methylene type isomer (CCH_2) lies about 45 kcal mol^{-1}higher in energy[107]. According to earlier computations, the linear (HAlCH) structure is not even a minimum on the $AlCH_2$ potential energy surface[98]. This has to do with the resistance of second-row elements to hybridization and the extent to which the fragment molecular orbitals' sizes match up for overlap[99].

CHAPTER 2

ALUMINUM FOILS: THE CONTRASTING CHARACTERS OF HYPERCONJUGATION AND STERIC REPULSION IN ALUMINUM DIMETALLOCENES[1]

[1]Compaan, K., Wilke, J., and Schaefer, H. 2011. *Journal of the American Chemical Society*, **133**, 13387–13396. Reprinted here with permission of publisher.

2.1 Abstract

The novel sandwich complex $Cp^*_2Al_2I_2$, which was recently synthesized by Minasian and Arnold, has been characterized using *ab initio* and density functional methods. A large family of related compounds was also investigated. Although a few Al(II)-Al(II) bonds are known, this is the first such bond to be supported by Cp type ligands. In addition, in the remarkable $Cp^*_4Al_4$ synthesis by Roesky $Cp^*_2Al_2I_2$ is the Al(II) intermediate; $Cp^*_4Al_4$ is important as a precursor to novel organoaluminum species. Halogen and ligand effects on the Al−Al bond in $Cp^*_2Al_2I_2$ were systematically explored by studying a series of twenty $Cp^*_2Al_2I_2$ derivatives using density functional theory with relativistic basis sets for the halogens. Comparison was made with the focal point treatment, which uses extrapolation to estimate the full configuration interaction, complete basis set limit energy. Torsional potential energy curves, natural population analyses, and enthalpies of hydrogenation were computed. Using the focal point approach, torsional barriers were computed with 0.05 kcal mol^{-1} uncertainty. The interplay of steric and electronic effects on the torsional potential energy curves, enthalpies of dehydrogenation reactions, and geometries is discussed. In species with small ligands (R=H, Me), hyperconjugative effects determine the torsional landscape, whereas steric repulsions dominate in species with Cp^* alkyl ligands. Species with Cp ligands represent an intermediate case, thus providing insight into how ligands modulate the structures and properties of small metal clusters.

2.2 Introduction

The pentamethylcyclopentadienyl aluminum tetramer ($[Cp^*Al]_4$) was the first Al(I) compound found to be stable at room temperature[60]. The tetramer (Figure 2.1) features four aluminum atoms arranged in a tetrahedron, each of which is η^5 coordinated to a Cp^* ring. $[Cp^*Al]_4$ has rich reactivity, so it is synthetically important as a precursor to aluminum-transition metal bonds[34–37], aluminum-boron donor-acceptor bonds[38], aluminum cluster complexes[39], and iminoalanes[40,41]. In 1998, Schormann and coworkers reported a new synthetic route to $[Cp^*Al]_4$ which, unlike the original method, does not require extreme temperatures[33]. The reaction scheme is shown in Figure 2.2. This method involves reduction of an Al(III) compound ($[Cp^*AlI(\mu I)]_2$); in 2008 Minasian and Arnold isolated the Al(II) intermediate, $Cp^*_2Al_2I_2$.[24]

The current study was inspired by Minasian and Arnold's unusual Al(II) sandwich complex. Its crystal structure is shown in Figure 2.3. Homonuclear bonding in group 13 elements has attracted much attention[25–27], particularly in the context of low-oxidation state main group chemistry. Several of the known molecules with Al−Al bonds are formally aluminum (II), but none of them has Cp-type ligands[28–32]. Moreover, surprisingly little is known about divalent aluminum[2], compared to its mono- and trivalent relatives[3,4]. Recent reviews highlight the importance of low-oxidation state aluminum in modern inorganic chemistry. The aluminum (I) analogs of N-heterocyclic carbenes are precursors to exotic bicyclo and spiro organoaluminum species[4]. Low valent aluminum compounds have been proposed as intermediates in radical and photochemical reactions[2]. Many low oxidation state aluminum compounds have only lately become accessible, due to improved methods for handling these typically air-sensitive complexes[2,3].

Molecules containing a non-metallic Al−Al bond are called dialanes, and are a recent synthetic achievement. The first dialane was made in 1988 by Werner Uhl[51]. The Al−Al

bond is 2.66 Å long, surrounded by four bis(trimethylsilyl)methyl ligands. Rather bulky ligands are apparently required to support an Al−Al bond, since such ligands prevent disproportionation to aluminum metal[53] or polymerization[52]. Dialanes exhibit rich chemical reactivity, with Al−Al distances ranging from 2.5 to 2.9 Å. Thus, non-metallic Al−Al bonds are generally shorter than the metallic Al−Al distance of 2.86 Å[1]. A few groups have succeeded in creating a one-electron $\pi-$bond in dialanes, typically in those containing large alkyl or silyl ligands[28,54–59]. The results are radical anions, with Al−Al bonds noticably shorter than in the parent compounds. Wright and coworkers made a putative Al−Al double bond in 2003, but were unable to isolate it[30], although it does undergo a Diels-Alder type reaction with toluene. Three years later, the same group synthesized a compound with confirmed Al−Al multiple bonding, and a compound containing a (possibly aromatic) Al_3 ring[31]. The subject of this study, $Cp^*_2Al_2I_2$, has an Al−Al distance of 2.52 Å and η^5 coordinated pentamethylcyclopentadienyl (Cp^*) ligands.

Since 1991, several derivatives of $[Cp^*Al]_4$ have been synthesized. A variety of ligands can support the tetrahedral Al_4 core, including cyclopentadienyl (Cp) derivatives[53,61], tBu$_3$SiAl[62,63], C(SiMe$_3$)$_3$[64], Si(SiMe$_3$)$_3$[65], and 2, 6-iPr$_2$C$_6$H$_3$N(SiMe$_3$)[66]. A nearly tetrahedral Al_4 core can be supported solely by hydrogen atoms in the gas phase[67]. Substituted versions of Al_4H_6 have also been recently synthesized[68]. Uhl reviewed the structure and reactivity of Al_4 clusters in 2004[69], noting their "particular bonding situation" and "aesthetic charm." The metal-metal bonding occurs through four highly delocalized molecular orbitals, formed from the lone-pair σ-orbitals of the monomers[69]. Only the cyclopentadienyl derivatives form π-bonds to aluminum; all others form σ-bonds[4]. Surprisingly, $Cp^*_4Al_4$ is stable to 140°C, while Cp_4Al_4 decomposes at -50°C[53]. The disproportionation of $Cp^*_4Al_4$ to metallic aluminum is hindered by a large barrier to formation of $Al_{50}Cp^*_{12}$[70], the core of which resembles metallic aluminum packing[49]. However, if the Cp^* ligands are replaced with

Cp, there is almost no barrier to formation of the Al_{50} cluster. This significant change in physical properties due to methylation is not yet well understood[53,70].

A number of organometallics containing clusters of aluminum atoms have been synthesized[39,42–50], including the mixed aluminum and carbon clusters called carbaalanes[47,48]. Aluminum clusters are of interest since their cores resemble metallic packing, and since they easily disproportionate to metallic aluminum.

Although large organometallics with Al−Al bonds are an important class of molecules, existing computational studies are limited. Several groups have performed computations on $[CpAl]_4$ and related species. Early studies investigated the bonding[62,71] and ^{27}Al NMR shifts[72] of AlX tetramers (X=H, F, Cl, Cp, SiH_3, $SiMe_3$, Si*t*Bu_3) at the SCF and MP2 levels of theory. When $[AlSitBu_3]_4$ was synthesized in 1998, experimental data was interpreted with the aid of DFT computations[63]. In 2008, the newly synthesized $[Al(C_5Me_4H)]_4$ was compared to $[Cp^*Al]_4$ and $[CpAl]_4$ using DFT results[53]. However, the remarkably disparate stabilities of $[Cp^*Al]_4$ and $[CpAl]_4$ mentioned above have yet to be explained[53]. Most recently, DFT computations were used to understand the bridged geometry of an Al−Al bond supported by phosphorus-based ligands (Al_2PtBu_4)[32,73], rather than a simple Al−Al bond between two R_2Al units.

The simplest dialane, Al_2H_4, has been the subject of in-depth computational studies. The global minimum for these six atoms is actually $AlH_4^-Al^+$[74], since aluminum is hypovalent and this arrangement best involves the formally unoccupied Al $3p_z$-orbitals. However, $H_2Al-AlH_2$ is of interest as the aluminum analog of ethylene, and because it has been isolated in solid hydrogen matrices[75,76]. Molecular orbitals were computed[79], and the global potential energy surface (PES) explored[74,77,78] in early studies. More recently, Szabó and coworkers investigated why $X_2Al-AlX_2$ (X= H, F, Cl, Br, I) species prefer perpendicular (D_{2d}) geometries to planar (D_{2h}) structures[80]. It should be noted that, like Al_2H_4, the

global minima for Al_2F_4 and Al_2Cl_4 are $AlX_4^-Al^+$ [73], although the $X_2Al{-}AlX_2$ geometry can be stabilized by donor groups[3].

Interestingly, Al_2H_4 has the largest rotational barrier in the $X_2Al{-}AlX_2$ series, despite having the smallest ligands. At the TZ2P BP86 level of theory, it is 1.8 kcal mol^{-1}, which is about three times larger than the barriers for halogenated species[80]. This is consistent with Schleyer's analysis of the analogous boron compounds, H_2B-BH_2 and Cl_2B-BCl_2, based on Hartree Fock molecular orbitals[108]. First, B-H hyperconjugation is more effective than B-Cl hyperconjugation in the planar forms. Second, π conjugation of the halogen lone pairs into the empty boron p-orbitals is only present in Cl_2B-BCl_2. Taken together, these effects account for the fact that the torsional barrier of H_2B-BH_2 is 10.5 kcal mol^{-1}, while Cl_2B-BCl_2's is only 1.9 kcal mol^{-1} [108]. Szabó and coworkers came to similar conclusions for Al compounds[80]. Thus, torsional analysis can give insight into the subtle interplay of steric and electronic effects.

In this study, we explore the torsional potential energy curves (PECs) of a series of dialanes, $XRAl{-}AlRX$ (R=H, Me, Cp, Cp*: X=H, F, Cl, Br, I), initially using density functional theory (DFT). Natural bond orbital (NBO) reactivity descriptors, including charges and hyperconjugation strengths, are computed, which should guide future synthesis of novel small metal clusters. In order to benchmark the DFT results, we carry out focal point analyses with correlation treatments as extensive as CCSD(T) (coupled cluster, singles, doubles, and perturbative triples) and basis sets as large as aug-cc-pVQZ.

2.3 Methods

2.3.1 Focal Point Analysis

Al_2H_4, $Al_2H_2F_2$, and $Al_2H_2Cl_2$ were characterized using coupled cluster singles and doubles (CCSD)[8–10], with perturbative triples (CCSD(T))[11], in conjunction with augmented

correlation-consistent polarized valence double, triple, and quadruple-ζ basis (aug-cc-pVDZ, aug-cc-pVTZ, and aug-cc-pVQZ)[109,110]. Focal point tables were constructed according to the prescription of Allen[12–15]. The Hartree-Fock energy change (ΔE_{HF}) was extrapolated to the complete basis set (CBS) limit, using[16,17]:

$$E_X = E_{CBS/HF} + (X+1)be^{-9\sqrt{X}}\,. \tag{2.1}$$

Here, X is the cardinal number of the basis set (*e.g.* X=2 refers to the aug-cc-pVDZ basis set), while $E_{CBS/HF}$ and b are fitting coefficients. Next, the correlation energy is extrapolated to the CBS limit with[18]

$$E_X = E_{CBS}^{corr} + bX^{-3}\,. \tag{2.2}$$

Again, E_{CBS}^{corr} and b are fitting coefficients. The energies and extrapolations are used to construct an incremented focal point table, in which the first column is the HF reaction energy and extrapolation to the CBS limit. Successive columns contain MP2, CCSD, and CCSD(T) corrections to the previous level of theory (*e.g.* δ[MP2]=ΔE_{MP2}-ΔE_{HF}), and extrapolations to the CBS limit. Thus, the final column ($\Delta E_{CCSD(T)}$) is given by

$$\Delta E_{CCSD(T)} = \Delta E_{HF} + \delta[\mathrm{MP2}] + \delta[\mathrm{CCSD}] + \delta[\mathrm{CCSD(T)}]\,. \tag{2.3}$$

The final focal point estimate of the reaction energy (ΔE_{FP}) is found in the bottom right corner of the table and corresponds to an estimate of $\Delta E_{CCSD(T)}$ extrapolated to the CBS limit. Focal point analysis gives a detailed understanding of the reaction energy convergence, with respect to both increasing basis set size (columns) and correlation treatment (rows). In addition, examination of the table can yield an estimate of the error bars associated with the final reaction energy.

In these computations, only valence electrons are correlated. Corrections for core correlation were computed by taking the difference between frozen-core and all-electron MP2 single point energies with cc-pCVTZ basis sets[111–113].

2.3.2 Natural Bond Orbital Analysis

Natural population analyses were performed using the NBO 5.0 package and the B3LYP density functional in QChem[114]. DZP basis sets were employed for Al, C, and H, while DZVP basis sets[115] were used for the halogens, since the NBO package is not compatible with partial use of pseudopotentials.

2.3.3 Computational Methods

$Cp^*_2Al_2I_2$, its derivatives, and its fragments were studied with density functional theory (DFT)[20]. We used B3LYP[21,22] with DZP basis sets[116] for hydrogen, carbon, and aluminum. For iodine, the Stuttgart-Dresden-Bonn (SDB) pseudopotential and matching basis set[117] were selected to account for relativistic effects, because an all-electron treatment was not feasible. SDB pseudopotentials and basis sets were selected for the smaller halogens to ensure consistent treatment. This computational approach is abbreviated DZP SDB B3LYP. A fine quadrature grid was employed, with 75 radial points and 302 angular. DFT and small basis CCSD(T) computations were carried out in the QChem 3.2 package[23]. Large basis CCSD(T) computations were performed with Molpro 2006.1[118]. The Natural Bond Orbital (NBO) 5.0 package was used for population analysis[119–122].

2.4 Results and Discussion

2.4.1 Geometric Structures

Comparison of computed geometries with experimental measurements provides an important benchmark for the theoretical methods employed. The minimum energy structure of $Cp^*_2Al_2I_2$ at the DZP SDB B3LYP level is in good agreement with the crystal structure; it is shown in Figure 2.4. The Al−Al distance of 2.56 Å agrees with the measured bond length of 2.53 Å, and the Cp^* rings are η^5 coordinated. The theoretical carbon to aluminum distances range from 2.18 to 2.38 Å around the ring, which compares very favorably with the experimental range of 2.17 to 2.34 Å. The Al-I distance is 2.72 Å at the DZP SDB B3LYP level of theory, while the measured value is 2.64 Å. However, the I-Al-Al-I torsional angle in the optimized structure is 107°, which disagrees with the crystal structure value of 91°. In order to resolve this point, the torsional PEC about the Al-Al bond was explored. The I−Al−Al−I dihedral angle was varied in 10° increments from the equilibrium value and all other structural parameters were allowed to relax. Changing the torsion angle to 90° only raises the energy by about 0.5 kcal mol^{-1}. This shallow torsional potential energy curve, and possible crystal packing effects, resolve the apparent disagreement with experiment. Thus, where crystal structures are available, good agreement with experiment should be achieved.

We investigated halogen and ligand effects on $Cp^*_2Al_2I_2$ by replacing the iodine atoms with bromine, chlorine, fluorine, or hydrogen atoms, and the Cp^* ligand with Cp, Me, or H. Each structure was independently optimized, and harmonic vibrational frequencies were computed to identify stationary points as minimum energy structures. The reported geometric parameters are for minimum energy geometries; see Table 2.1 for a summary of the results. All of the structures considered here are closed-shell singlets, with HOMO-LUMO gaps of at least 4 eV.

If the alkyl ligand is H or Me, the Al−Al bond length decreases with increasing weight of X, from 2.579 Å in Al_2H_4 to 2.561 Å in $Al_2H_2I_2$, and from 2.596 Å in $Al_2Me_2H_2$ to 2.568 Å in $Al_2Me_2I_2$. The less electronegative larger halogens donate electrons to the empty 3p orbital on aluminum. This can be seen in the natural populations of the aluminum $3p_z$ orbital, shown in Table 2.2. Note that all species are in C_{2h} symmetry for this analysis, to make the axes and orbitals unambiguously identifiable. The occupation of this formally empty $3p_z$ orbital increases steadily with increasing halogen size, increasing the double bond character of the Al−Al interaction, and shortening the bond.

However, the bond length ordering changes significantly with larger alkyl ligands. In the Cp series, the Al−Al distance increases with increasing halogen weight, from fluorine (2.492 Å) to iodine (2.508 Å). Hydrogen substituted $Cp_2Al_2H_2$ has the longest Al−Al distance in the series (2.518 Å). The trend becomes clear in the Cp^* series; the Al−Al distance increases from 2.527 Å in $Cp^*_2Al_2H_2$ to 2.564 Å in $Cp^*_2Al_2I_2$. A graphical summary of these trends is presented in Figure 2.5.

Torsional PEC's were computed for all structures by varying the X−Al−Al−X dihedral angle in 10° increments and allowing all other parameters to relax. These are displayed in Figure 2.6 through Figure 2.9. We find the largest torsional barriers in $H_2Al_2X_2$ and $Me_2Al_2X_2$ for X = H. If X is a halogen, the PEC is very flat between 110° and 250°, changing by less than 0.35 kcal mol^{-1} for $H_2Al_2X_2$ and less than 0.10 kcal mol^{-1} for $Me_2Al_2X_2$. By way of illustration, Al_2H_4 has a barrier of 2.0 kcal mol^{-1}, versus only 0.3 kcal $mol^{-1}$for $Al_2H_2I_2$. Similarly, $Me_2Al_2H_2$'s barrier is 1.0 kcal mol^{-1}, versus 0.1 kcal mol^{-1} for the iodine version. This is in line with previous work on Al_2X_4 species[80].The large barriers for hydrogen-substituted dialanes are due to hyperconjugation in the twisted geometry and the absence of conjugations or hyperconjugations in the planar form. The barriers decrease when X is a halogen, because the lone pairs overlap favorably with the empty Al $3p_z$ orbital in the planar form, as shown in Table 2.2 and discussed below. This offsets the loss of hyperconjugation,

lowers the internal rotational barrier[80], and explains the nonintuitive ordering of barrier heights in $H_2Al_2X_2$ and $Me_2Al_2X_2$.

Interestingly, the rotational barriers in $Cp^*_2Al_2X_2$ and $Cp_2Al_2X_2$ generally increase with the mass of the halogen, while hydrogen falls between fluorine and chlorine. The largest barrier in each series corresponds to iodine; $Cp_2Al_2I_2$ (4 kcal mol^{-1}) and $Cp^*_2Al_2I_2$ (10 kcal mol^{-1}). Torsional barriers are plotted against halogen substituent in Figure 2.10. Although the general trends seen in the small alkyl substituents reverse with Cp and Cp* species, those with fluorine consistently have smaller rotational barriers than those with hydrogen. Thus, even in large molecules, hyperconjugation seems to determine the ordering of the rotational barriers for the fluorine and hydrogen substituted systems. As seen in Table 2.3, the Al−Al bond lengthens more with larger alkyl groups and larger halogens. This may indicate that steric effects are more significant than hyperconjugation when large alkyl groups and heavy halogens are present. Further evidence for this explanation is given in Figure 2.11. Here, the population of the $3p_z$ orbital on aluminum is plotted against halogen substituent for all four series of alkyl ligands. The formally empty $3p_z$ orbital on aluminum was identified as the formally unoccupied lone-pair (LP*) natural bond orbital with the largest p-character (over 90%), and largest population. Since NBO assigns two-center bonds, it gives an incomplete description of aromatic rings like Cp. Thus, it assigned as many as three partially-occupied non-Lewis orbitals with some $3p_z$ character to aluminum in the Cp and Cp* series. This is not a significant problem, since we are primarily interested in the Al−Al bond. Figure 2.11 clearly shows that the larger halogens are better donors to the empty $3p_z$ orbital on aluminum. However, competing steric effects cause the trends followed in the small species to reverse in species with Cp and Cp* alkyl ligands.

While most of the potential curves are smooth, the PEC for $Cp^*_2Al_2H_2$ oscillates. The bumps correspond to abrupt changes in the Cp* hapticity. $Cp^*_2Al_2H_2$ has η^5 hapticity below 30° and between 140° and 180°. Between 40° and 130° it is η^2. This is evidenced by

sharp changes in the range of Al-C_{ring} distances, while the Al−Al and Al−H distances are essentially unchanged. In general, Cp^* rings have higher hapticity than Cp rings, evidenced by narrower ranges of ring-carbon to aluminum distances (Table 2.1). The hapticity also increases with increasing halogen size; for example, the Cp^* hapticity increases from two in $Cp^*_2Al_2H_2$ to five in $Cp^*_2Al_2I_2$. Consistent with these two trends, $Cp^*_2Al_2I_2$ has the narrowest range of ring-carbon to aluminum distances (2.184−2.375 Å), while $Cp_2Al_2H_2$ has the largest range (2.155−3.106 Å).

In order to estimate the Al−Al bond strength, 0 K enthalpies of dehydrogenation of hydrogen-capped monomers were computed using harmonic zero point energies. The monomers' geometries were optimized independently, and the changes in enthalpy were computed for the following reactions:

$$2\ H_2AlX \rightarrow H_2Al_2X_2 + H_2$$
$$2\ MeAlHX \rightarrow Me_2Al_2X_2 + H_2$$
$$2\ Cp^*AlHX \rightarrow Cp^*_2Al_2X_2 + H_2$$
$$2\ CpAlHX \rightarrow Cp_2Al_2X_2 + H_2$$

The dehydrogenation enthalpy results are summarized in Table 2.4 and Figure 2.12. Examination of the results for alkyl ligands H and Me reveals that the shorter Al−Al bonds correspond to larger dehydrogenation energies. In both series, the Al−Al distance decreases down the series, and the ΔH_{rxn} also decreases. This trend is not followed in the Cp series; the enthalpies of dehydrogenation for F, Cl, Br, and I substituted species are all nearly −3 kcal mol^{-1}. However, the hydrogen substituted version has a +1 kcal mol^{-1} enthalpy of dehydrogenation. The picture is somewhat clearer in the Cp^* series; with the exception of the H substituted species, the enthalpy of dehydrogenation increases with lengthening bond distance. The $Cp^*_2Al_2H_2$ does not fit the trend, since it has η^2 Cp^* rings, while the others have η^5 ligands. Thus, as in the discussions of Al−Al distances and rotational barriers,

the Cp series represents the crossover from electronic effects dominating in the small alkyl ligands (H, Me) to steric effects, which dominate in the Cp^* series. A graphical summary is presented in Figure 2.12.

2.4.2 NBO Descriptors

The NBO donor-acceptor paradigm provides a powerful conceptual framework for understanding the subtle hyperconjugative effects in Al_2X_4 species, particularly those involving the formally unoccupied $3p_z$ orbitals on Al. NBO quantifies qualitative bonding concepts, such as hyperconjugation, charge transfer, and other donor-acceptor interactions, including dative coordination. This approach reveals why DFT methods overestimate the torsional barrier in Al_2H_4 compared to highly accurate correlated methods (see next section). The atomic $3p_z$ population on aluminum was computed at various levels of theory, both at the flat D_{2h} and twisted D_2 DZP B3LYP geometries. With each method shown in Table 2.11 the $3p_z$ populations are very similar at the D_{2h} geometry. However, both B3LYP and BP86 are overly delocalized at the D_2 geometry. The extent to which DFT functionals overestimate the torsional barrier is closely related to how much they overestimate the $3p_z$ population at the D_2 geometry, compared with the aug-cc-pVTZ HF result. Although the population differences are rather small, delocalization is a strong energy lowering effect and could certainly account for the difference in barrier heights. The extra delocalization in the DFT results (amounting to about 0.005 electrons per aluminum atom, and 0.01 electrons total) could account for up to a 6 kcal mol^{-1} difference in the barrier heights.

The energy lowering (ΔE) due to mixing occupied orbital (ϕ_i) with unoccupied orbital (ϕ_{j*}) can be calculated using second order perturbation theory. In NBO terms, ϕ_i and ϕ_{j*} are rigorously localized one or two center orbitals, and ΔE describes the energy benefit of their mixing to form a rigorously doubly-occupied orbital. $F_{i,j*}$ is the Fock matrix element

between the two orbitals, and ϵ_i and ϵ_{j*} are the respective orbital energies[123].

$$\Delta \mathrm{E} = 2\frac{F_{i,j*}^2}{\epsilon_i - \epsilon_{j*}} \tag{2.4}$$

The number of electrons (q) transferred from ϕ_i to ϕ_{j*} can be approximated by

$$q = 2\frac{F_{i,j*}^2}{(\epsilon_i - \epsilon_{j*})^2}\,. \tag{2.5}$$

An approximation for the energy lowering due to orbital mixing/charge transfer is given by[124,125]:

$$q \times (\epsilon_i - \epsilon_{j*}) = \Delta \mathrm{E}\,. \tag{2.6}$$

The orbital energy differences involved are on the order of 1 Hartree; in the $Al_2H_2X_2$ series the orbital energy difference between the lone-pairs on the halogen and the formally empty 3p orbital on aluminum range from 0.27 a.u. (X=Cl) to 0.93 a.u. (X=Br). In the largest system, $Cp^*_2Al_2I_2$, the lone pairs on iodine are 0.97 a.u. lower in energy than the empty 3p orbital on aluminum. Thus, the above equation can be further approximated as

$$q \approx \Delta \mathrm{E}\,. \tag{2.7}$$

In this equation, q is the number of electrons and ΔE is in Hartrees. (These equations assume that the orbitals mix to a small extent, and thus the original orbitals are not strongly perturbed by the interaction.) Thus, the transfer of 0.01 electrons is worth about 6 kcal mol^{-1}. From Table 2.11, this extra delocalization is not isolated to the B3LYP functional.

The energy lowering due to delocalization can be further dissected into contributions from particular bonds; this is found in the E2PERT table of the NBO output. In twisted Al_2H_4 at

the DZP B3LYP level, each Al−H bond hyperconjugates with the formally empty 3p orbital on the neighboring aluminum atom. Each interaction is worth about 1.34 kcal mol^{-1}, for a total of 5.36 kcal mol^{-1}. This is reasonably similar to the above estimate of 6 kcal mol^{-1}. The Al−H to 3p hyperconjugation is absent in planar Al_2H_4, and since it occurs across the Al−Al bond in twisted Al_2H_4, it contributes to the torsional barrier.

Similar reasoning can be applied to the torsional barrier in $Al_2H_2F_2$, which is +0.26 kcal mol^{-1} at the DZP SDB B3LYP level of theory but less than 1 cm^{-1} using cc-pVDZ CCSD(T) geometries and energies (see next section). Examination of the NBO output at the DZVP B3LYP level reveals that hyperconjugation is greatly reduced in $Al_2H_2F_2$, due to the very polarized Al−F bonds. In both the planar and twisted geometries, donation from the Al−F bond to 3p on the neighboring aluminum is worth less than 0.10 kcal mol^{-1}, and does not appear in the NBO output. Lone pairs on fluorine interact significantly with the 3p orbital on the closest aluminum atom. However, this vicinal conjugation is virtually unaffected by twisting the molecule, and thus does not contribute to the rotational barrier. Two kinds of delocalization occur in twisted $Al_2H_2F_2$ which are absent in the planar form. There is a slight donation (0.13 kcal mol^{-1}) from a fluorine lone pair to the opposite aluminum 3p orbital. Finally, donation from the Al−H bond is significantly reduced, compared to Al_2H_4; each interaction is worth only 0.63 kcal mol^{-1}. The above discussion of Al_2H_4 indicates that B3LYP tends to overestimate delocalizations, so it is not unreasonable that the very small rotational barrier in $Al_2H_2F_2$ disappears with the more accurate CCSD(T) method. This possibly warrants further investigation. However, we demonstrated above that B3LYP reproduces trends for these systems, and is a suitable level of theory for this study; although the rotational barriers tend to be overestimated, the trends are reproduced correctly.

The natural charges on the halogen atoms were consistent over all the structures; see Table 2.5. The natural charge residing on aluminum is shown in Table 2.6. It is evident that characterizing $Cp^*_2Al_2I_2$ as an Al(II) complex is somewhat misleading. Since Al is less

electronegative than C, H, or any halogen, all ligands are formally assigned a -1 charge, leaving Al with a formal $+2$ charge. However, the ligand natural charges are all closer to -0.5 than to -1 (Table 2.7). The natural charge on aluminum is only $+1$ in $Cp^*_2Al_2I_2$ and not larger than $+1.4$ in any of the molecules considered. The ligands participate in donor-acceptor interactions with the $3p_z$ orbital on Al, preventing a large natural charge from accumulating on the metal atoms.

2.4.3 Focal Point Analysis and Structural Benchmarks

To evaluate the reliability of the B3LYP treatments, energies, structural parameters, and harmonic vibrational frequencies were computed for the parent Al_2H_4 and its dissociation to AlH_2. (Full results are provided in the supplementary information.) In general, B3LYP is in excellent agreement with CCSD(T) for these systems, with bond lengths within 0.02 Å, angles within 0.6°, and frequencies within 18 cm^{-1}. There are a few notable exceptions; the B3LYP dissociation energy for Al_2H_4 is 4.2 kcal mol^{-1} too low, and the torsional mode (ν_1) for Al_2H_4 is overestimated by about 40% (46 cm^{-1}) at the DZP B3LYP level of theory. Finally, the rotational barrier is 1 kcal mol^{-1} too high. A previous study on ethane and its analogs (C_2H_6, Si_2H_6, $SiGeH_6$, and Ge_2H_6) found that B3LYP underestimates their rotational barriers by about 10%, while CCSD(T) may overestimate them[126]. However, focal point analysis of the Al_2H_4 barrier (Table 2.8) indicates that the CCSD(T) estimate is well converged with respect to theory and basis set. The CCSD(T) increment is 0.07 kcal mol^{-1}. Subsequent corrections are expected to be much smaller, since quadruple excitations contribute less than triple excitations. Changing the basis set from aug-cc-pVTZ to aug-cc-pVQZ only changes the CCSD and CCSD(T) increments by 0.01 kcal mol^{-1}, indicating that cc-pVQZ is a close approximation to the CBS limit for this system. Thus, the uncertainty in the final estimate (ΔE_{FP}) is on the order of 0.05 kcal mol^{-1}. B3LYP overestimates the torsional barrier in this molecule. Physical reasons for this are discussed below.

Focal point tables were also computed for the torsional barriers in $Al_2H_2F_2$, $Al_2H_2Cl_2$, and $Al_2H_2Br_2$. The rotational barriers converged very quickly, both with respect to correlation and basis set. The uncertainty is on the order of 0.05 kcal mol^{-1}. Core corrections to the rotational barriers were found to be negligible. These results are compared to the DZP B3LYP barriers in Table 2.9, and full focal point tables are provided in the supplementary information. Physical insight into why DFT overestimates the torsional barrier in $Al_2H_2F_2$ is provided by NBO analysis. (See previous section.)

To further benchmark the DFT results, we carried out focal point analysis on the following reactions:

$$2\ AlH_3 \rightarrow Al_2H_4 + H_2$$

$$2\ AlH_2F \rightarrow Al_2H_2F_2 + H_2$$

$$2\ AlH_2Cl \rightarrow Al_2H_2Cl_2 + H_2$$

$$2\ AlH_2Br \rightarrow Al_2H_2Br_2 + H_2$$

The core-corrected focal point reaction energies are compared to DFT results in Table 2.10; full focal point tables are provided in the supplementary information. The reaction energies converged more slowly to the CBS FCI limit than the torsional barriers did, and the uncertainty in the final ΔE_{FP} is approximately 0.5 kcal mol^{-1}. Although DZP SDB B3LYP overestimates the torsional barriers and reaction energies, the trends are reproduced correctly. These results indicate that DZP B3LYP is a suitable level of theory for a qualitative study of Al−Al bonding. While CCSD(T) is the "gold-standard" for computational chemistry, B3LYP is currently a necessity for large systems like $Cp^*_2Al_2I_2$.

2.5 Concluding Remarks

We have completed a systematic study of aluminum dimetallocenes using *ab initio* and density functional methods. This is an exciting new class of organoaluminum molecules, the first

of which ($Cp^*_2Al_2I_2$) was recently synthesized by Minasian and Arnold. Electronic effects, such as hyperconjugation, were found to be crucial in the small $Al_2R_2X_2$ (R=H, Me) species. NBO analysis shows clear relationships between hyperconjugative interactions, torsional barrier heights, and Al−Al bond lengths. However, these trends are reversed in species with Cp^* ligands, with Cp being an intermediate case. NBO analysis is especially useful in this regard, because it connects electronic structure theory to a chemically intuitive picture of bonding. This research should provide deeper insight into novel aluminum organometallics, provide computational benchmarks for such molecules, and guide future synthesis efforts.

2.6 Supporting Information Available

Complete data tables, coordinates and energies for optimized structures, and complete references 86 and 87 are available in the supplementary data. This information is available free of charge via the Internet at http://pubs.acs.org/.

2.7 Acknowledgements

This research was supported by the U. S. National Science Foundation, Grant CHE 0749868. The authors thank Andy Simmonett, Lucas Speakman, and Francesco Evangelista for helpful discussions.

2.8 Tables

Structure	Halogen	r(Al-Al)	r(Al-X)	τ(X-Al-Al-X)	r(Al-ligand)	Hapticity
$Cp^*_2Al_2X_2$	H	2.527	1.607	137.8	$2.136 - 3.002$	2
	F	2.537	1.731	166.1	$2.178 - 2.376$	5
	Cl	2.549	2.266	120.7	$2.169 - 2.420$	5
	Br	2.560	2.447	113.4	$2.177 - 2.405$	5
	I	2.564	2.719	107.0	$2.184 - 2.375$	5
$Cp_2Al_2X_2$	H	2.518	1.594	127.7	$2.155 - 3.106$	2
	F	2.492	1.700	138.4	$2.129 - 2.880$	2
	Cl	2.499	2.185	116.9	$2.121 - 2.909$	2
	Br	2.506	2.342	112.7	$2.125 - 2.917$	2
	I	2.508	2.584	110.7	$2.123 - 2.916$	2
$Me_2Al_2X_2$	H	2.596	1.596	92.0	1.970	
	F	2.585	1.694	180.0	1.947	
	Cl	2.580	2.166	160.0	1.947	
	Br	2.578	2.317	138.4	1.950	
	I	2.568	2.549	120.1	1.951	
$H_2Al_2X_2$	H	2.579	1.589	90.1	1.589	
	F	2.575	1.687	112.1	1.577	
	Cl	2.569	2.152	109.9	1.575	
	Br	2.568	2.299	110.2	1.576	
	I	2.561	2.525	109.8	1.576	

Table 2.1: Optimized structural parameters for $Cp^*_2Al_2I_2$ and several related complexes. Structural parameters are in Å and degrees. The Al-ligand distances are measured to ring-carbon atoms for Cp groups and to the appropriate carbon atom for methyl groups.

	Alkyl Ligand	
Halogen	H	Me
H	0.001	0.018
F	0.061	0.070
Cl	0.093	0.102
Br	0.107	0.114
I	0.127	0.132

Table 2.2: Out-of-plane Al $3p_z$ atomic orbital populations (e) for C_{2h} geometries of selected dialanes at the DZVP B3LYP level of theory.

		Alkyl Ligand			
		H	Me	Cp	Cp*
Halogen	H	1.05%	0.85%	0.68%	1.62%
	F	0.19%	0.00%	0.52%	0.16%
	Cl	0.31%	0.04%	1.60%	2.39%
	Br	0.31%	0.16%	1.84%	3.13%
	I	0.43%	0.39%	2.31%	4.33%

Table 2.3: Lengthening of Al−Al bond during torsion from equilibrium to τ(X−Al−Al−X) = 180°.

Structure	Halogen	ΔH_{rxn} (kcal mol^{-1})	r(Al-Al) (Å)	Hapticity
$Cp^*_2Al_2X_2$	H	+6.4	2.527	2
	F	−2.1	2.537	5
	Cl	+0.1	2.549	5
	Br	+0.9	2.560	5
	I	+1.0	2.564	5
$Cp_2Al_2X_2$	H	+1.2	2.518	2
	F	−2.5	2.492	2
	Cl	−2.6	2.499	2
	Br	−2.5	2.506	2
	I	−3.1	2.508	2
$Me_2Al_2X_2$	H	+7.7	2.596	
	F	+4.4	2.585	
	Cl	+3.5	2.580	
	Br	+3.2	2.578	
	I	+1.9	2.568	
$H_2Al_2X_2$	H	+6.3	2.579	
	F	+5.5	2.575	
	Cl	+4.6	2.569	
	Br	+3.8	2.568	
	I	+2.5	2.561	

Table 2.4: 0 K enthalpies of dehydrogenation for Al-Al species from hydrogen-capped monomers at the DZP SDB B3LYP level.

Structure	Ligand			
	H	Me	Cp	Cp*
$Al_2R_2H_2$	−0.37	−0.39	−0.38	−0.40
$Al_2R_2F_2$	−0.75	−0.76	−0.75	−0.76
$Al_2R_2Cl_2$	−0.55	−0.56	−0.55	−0.58
$Al_2R_2Br_2$	−0.47	−0.49	−0.47	−0.52
$Al_2R_2I_2$	−0.35	−0.38	−0.35	−0.43

Table 2.5: Halogen natural charges at the DZVP B3LYP level of theory.

Halogen	Ligand			
	H	Me	Cp	Cp*
H	0.73	0.98	0.94	1.00
F	1.16	1.37	1.33	1.40
Cl	0.92	1.14	1.08	1.17
Br	0.84	1.07	1.00	1.11
I	0.70	0.94	0.87	1.00

Table 2.6: Aluminum natural charges at the DZVP B3LYP level of theory.

Halogen	Ligand			
	H	Me	Cp	Cp*
H	−0.37	−0.59	−0.56	−0.60
F	−0.41	−0.61	−0.58	−0.64
Cl	−0.37	−0.58	−0.53	−0.59
Br	−0.36	−0.58	−0.53	−0.59
I	−0.35	−0.57	−0.51	−0.57

Table 2.7: Ligand natural charges at the DZVP B3LYP level of theory, computed as the difference between the NPA of aluminum and that of the halogen.

	ΔE_{HF}	$+\delta$[MP2]	$+\delta$[CCSD]	$+\delta$[CCSD(T)]	$\Delta E_{CCSD(T)}$
aug-cc-pVDZ	+0.81	+0.21	−0.05	+0.05	[+1.02]
aug-cc-pVTZ	+0.88	+0.23	−0.08	+0.06	[+1.09]
aug-cc-pVQZ	+0.84	+0.21	−0.07	+0.07	[+1.04]
CBS LIMIT	[+0.84]	[+0.19]	[−0.07]	[+0.07]	[+**1.03**]
Fit	$a + (X+1)be^{-9\sqrt{X}}$	$a + bX^{-3}$	$a + bX^{-3}$	$a + bX^{-3}$	

Table 2.8: Focal point analysis of the torsional barrier for Al_2H_4 in kcal mol^{-1}. Energies were computed at DZP B3LYP geometries.

Halogen	Focal Point Barrier	DZP SDB B3LYP Barrier
H	$+1.03^a$	+2.08
F	$< 0.01^b$	+0.26
Cl	$+0.13^a$	+0.30
Br	$+0.23^a$	+0.24

Table 2.9: Comparison of DFT torsional barriers (kcal mol^{-1}) in $Al_2H_2X_2$ species to focal point results.
[a] DZP SDB B3LYP geometries. [b] cc-pVDZ CCSD(T) geometries. See supplemental information.

Halogen	Core Corrected Focal Point ΔE_{rxn}	DZP B3LYP ΔE_{rxn}
H	+3.55	+7.1
F	+4.42	+6.7
Cl	+2.79	+5.8
Br	+1.88	+5.0

Table 2.10: Comparison of focal point reaction energies (kcal mol^{-1}) of $2AlH_2X \rightarrow Al_2H_2X_2 + H_2$ to DFT results.

	Level of Theory			
Property	aug-cc-pVTZ HF	DZP HF	DZP B3LYP	DZP BP86
D_{2h} 3p occ.	0.0008	0.0007	0.0007	0.0007
D_2 3p occ.	0.0045	0.0058	0.0123	0.0170
Barrier (kcal mol^{-1})	0.88	1.59	2.08	2.38

Table 2.11: Aluminum 3p populations and rotational barriers for Al_2H_4.

2.9 Figures

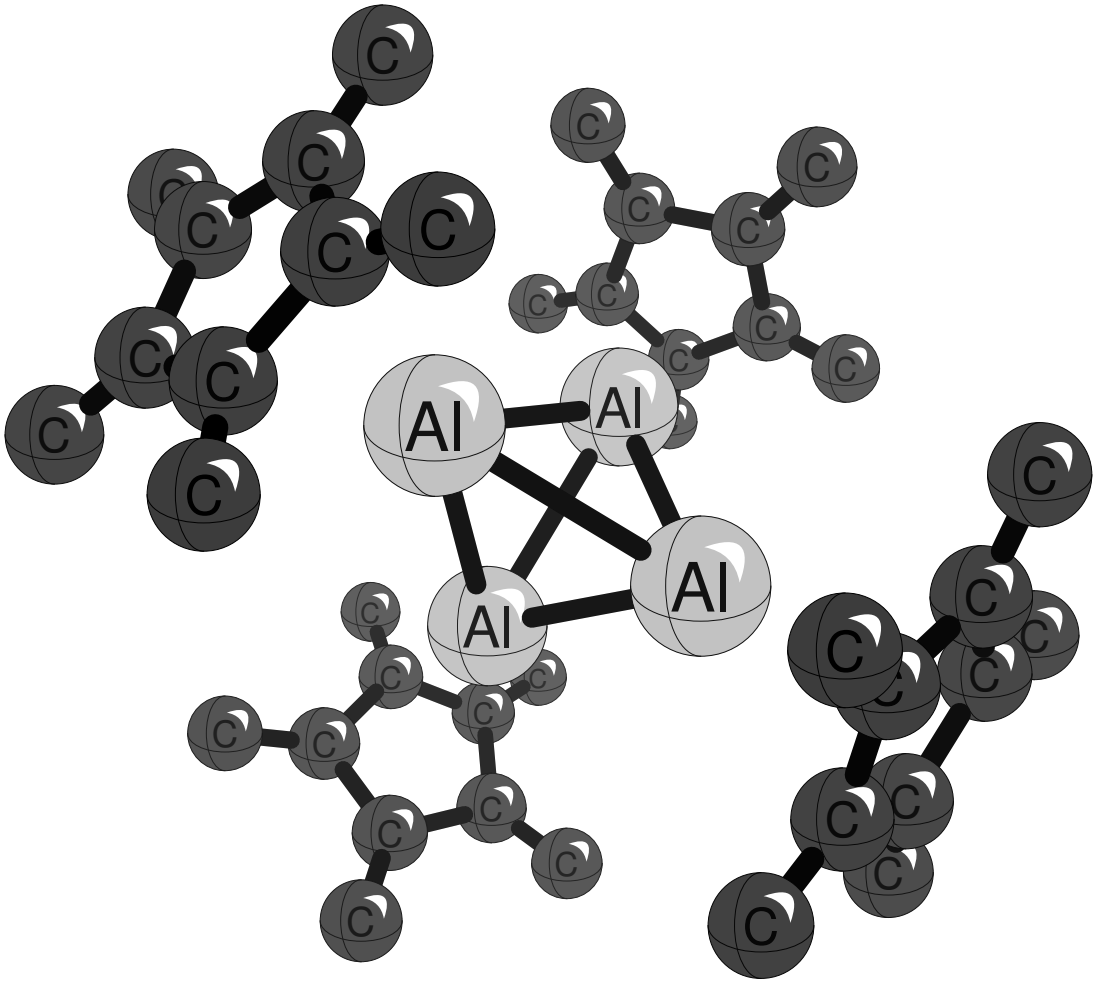

Figure 2.1: Crystal structure of Schnöckel and coworkers[60] for pentamethylcyclopentadienyl aluminum(I) tetramer. Hydrogen atoms have been omitted for clarity.

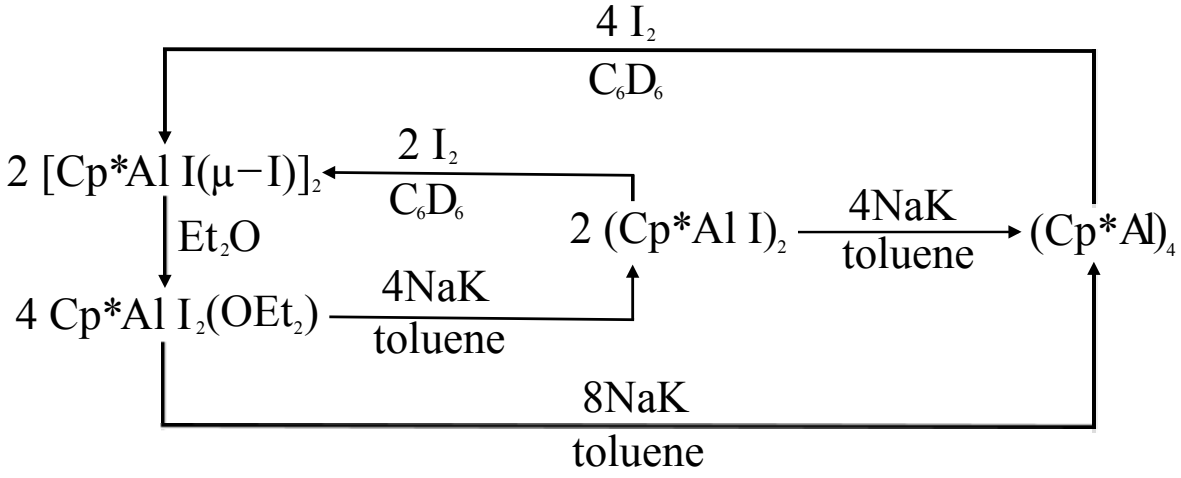

Figure 2.2: Experimental synthetic pathway to $[Cp^*Al]_4$ involving $Cp^*_2Al_2I_2$[60]

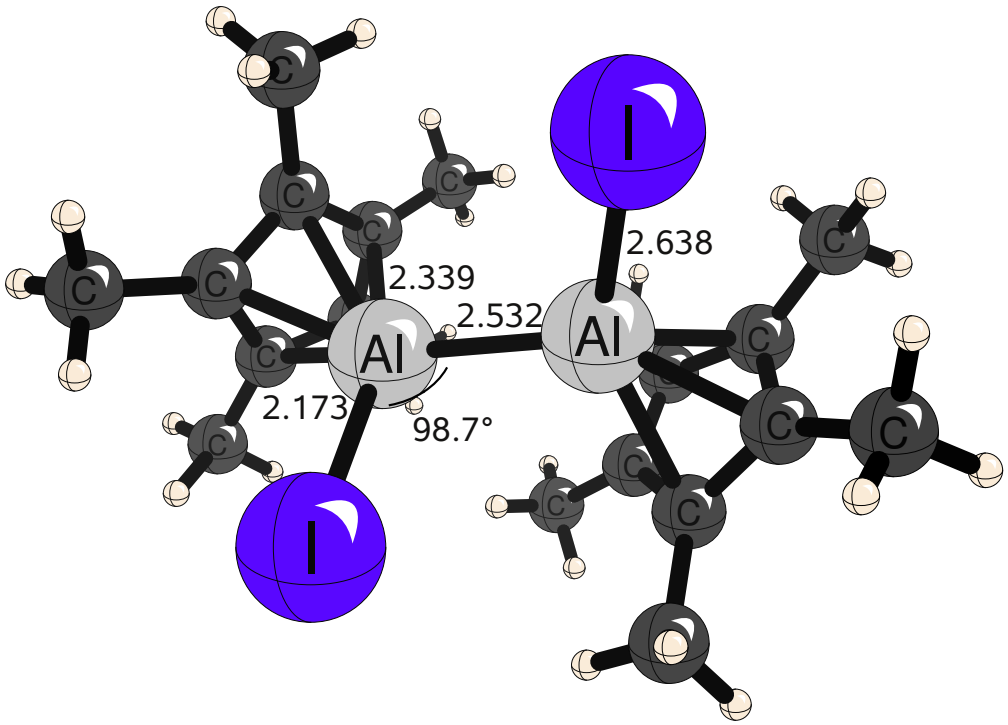

Figure 2.3: Crystal structure of Minasian and Arnold[24] for bis-pentamethylcyclopentadienyl diiododialane.

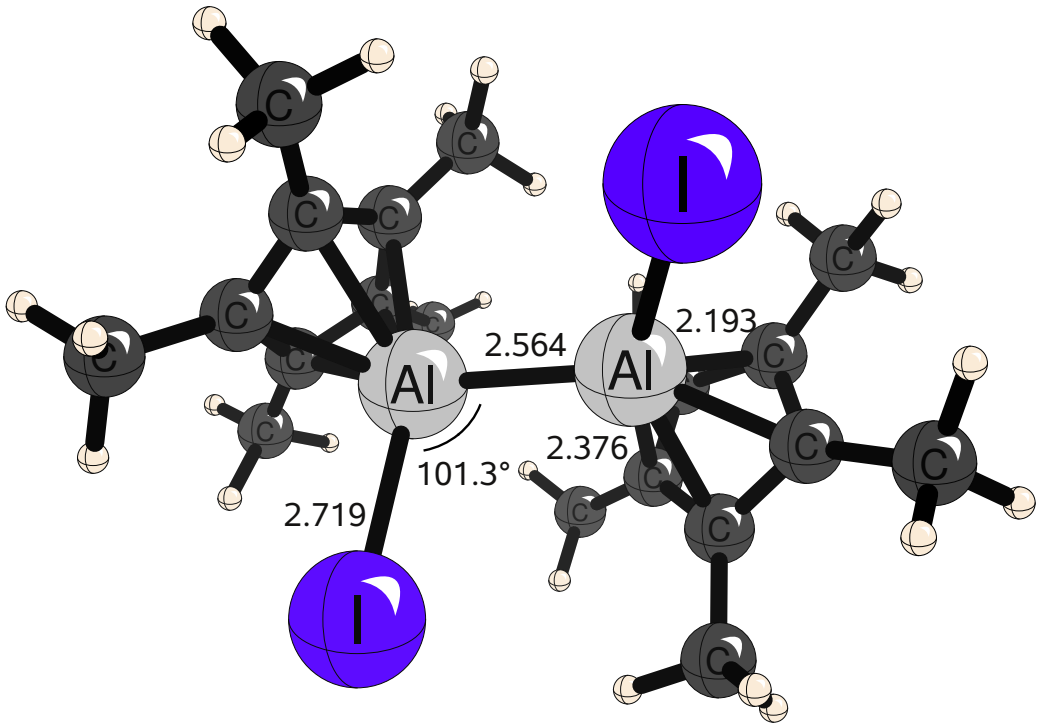

Figure 2.4: Theoretical geometry of Minasian and Arnold's compound[24] $Cp^*_2Al_2I_2$ at the DZP SDB B3LYP level of theory.

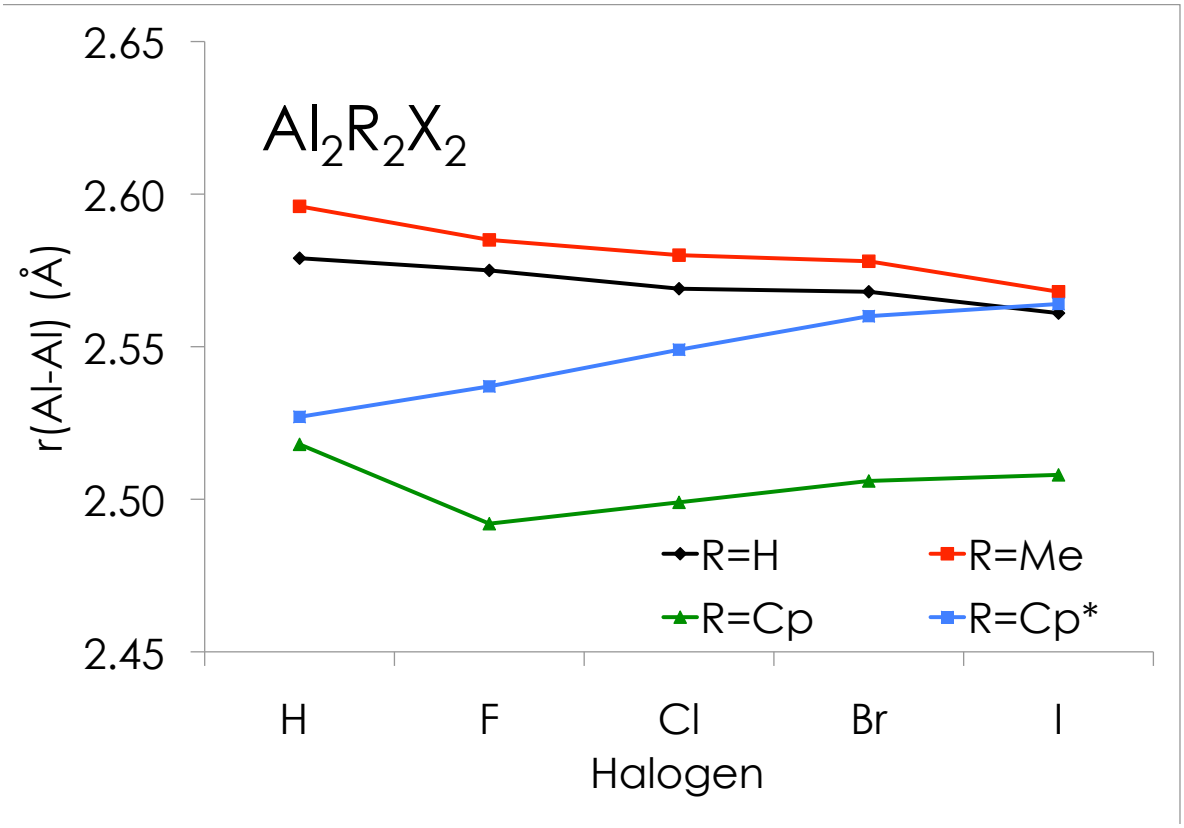

Figure 2.5: The Al−Al distance plotted against halogen substituent in aluminum dimetallocenes at the DZP SDB B3LYP level of theory.

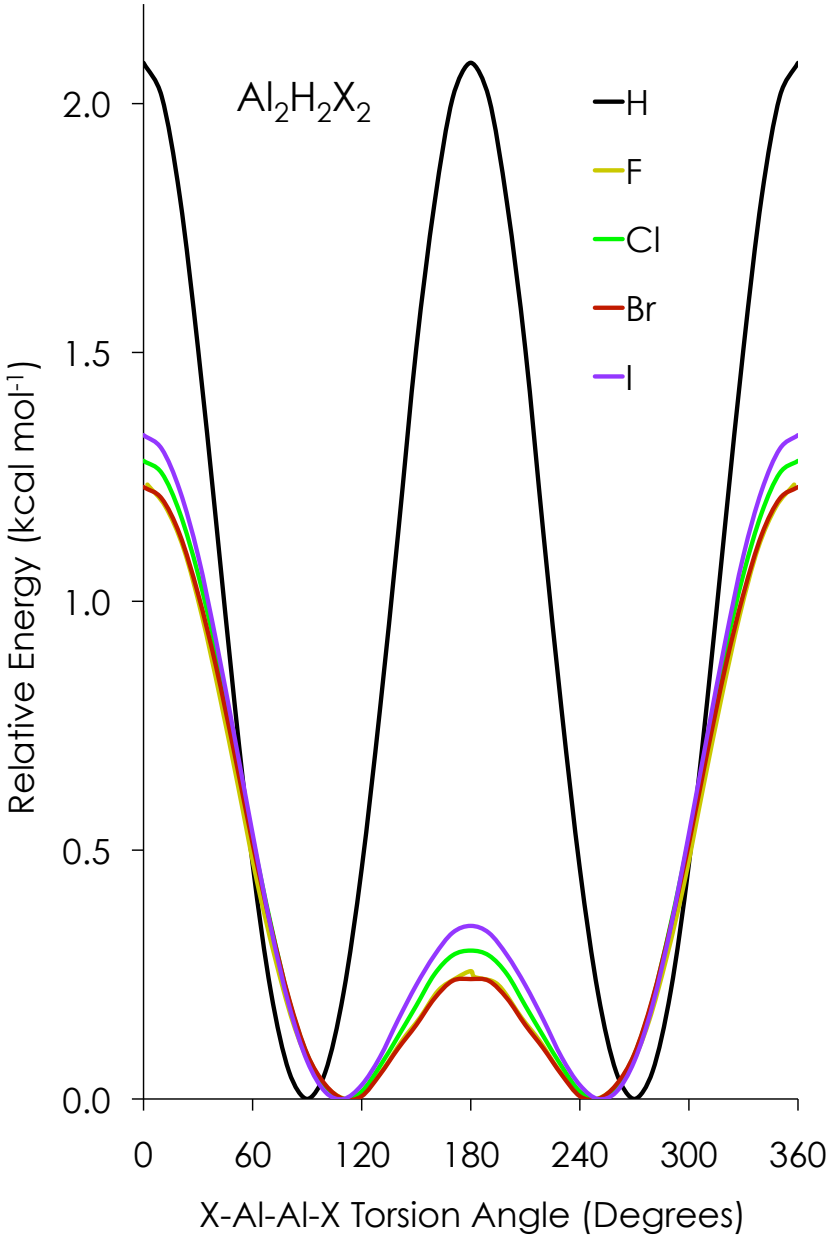

Figure 2.6: Torsional potential energy curves for $Al_2H_2X_2$ at the DZP SDB B3LYP level of theory.

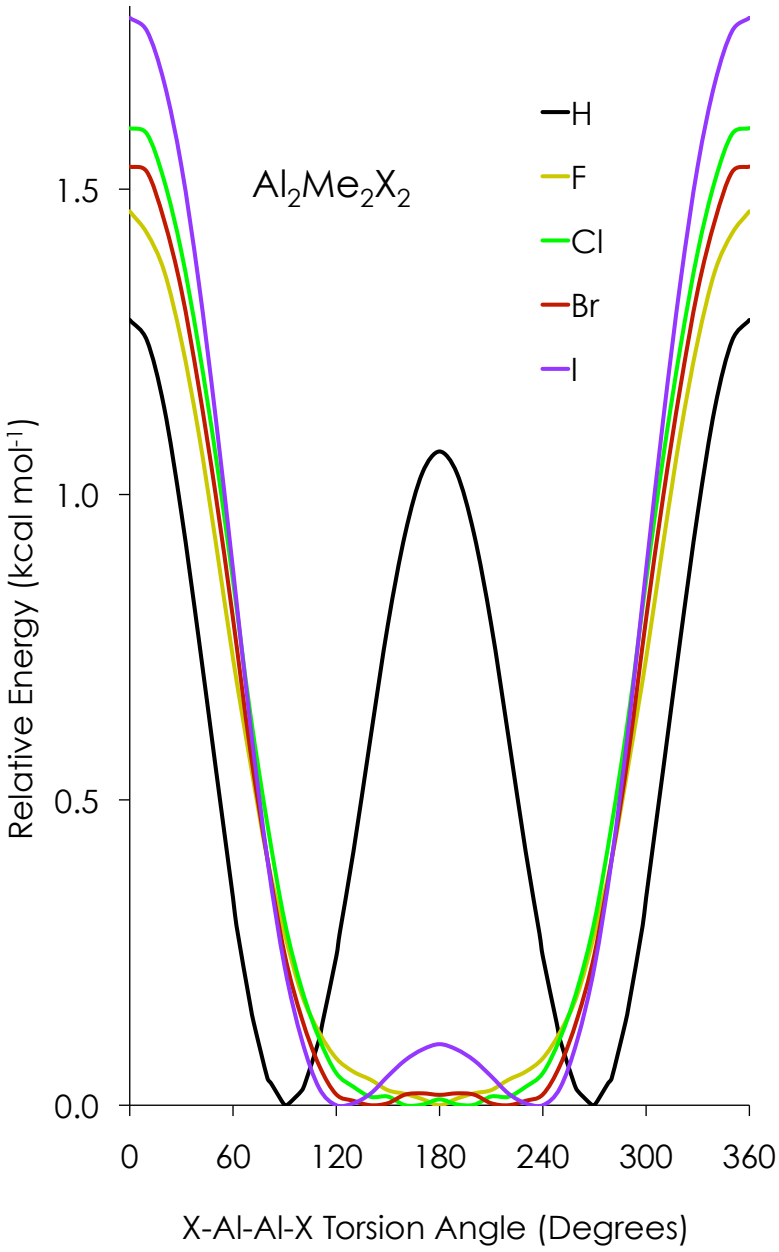

Figure 2.7: Torsional potential energy curves for $Al_2Me_2X_2$ at the DZP SDB B3LYP level of theory.

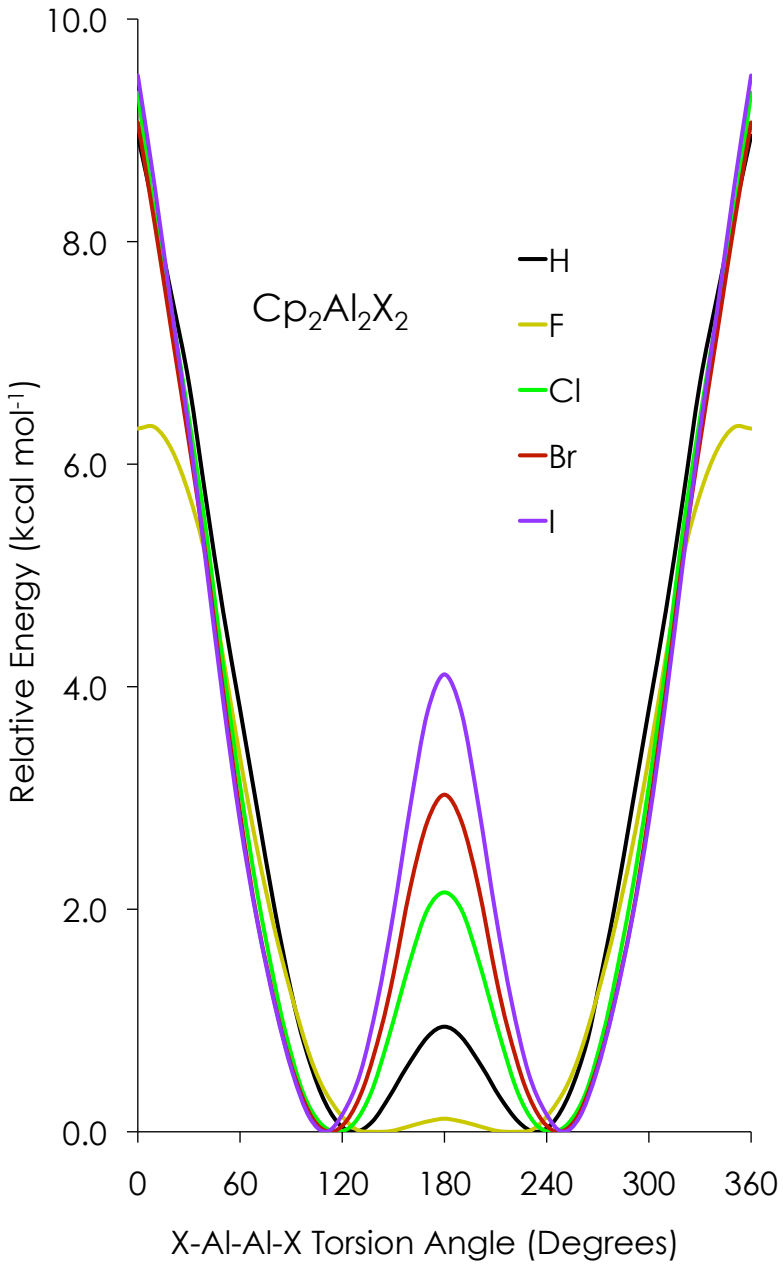

Figure 2.8: Torsional potential energy curves for $Cp_2Al_2X_2$ at the DZP SDB B3LYP level of theory.

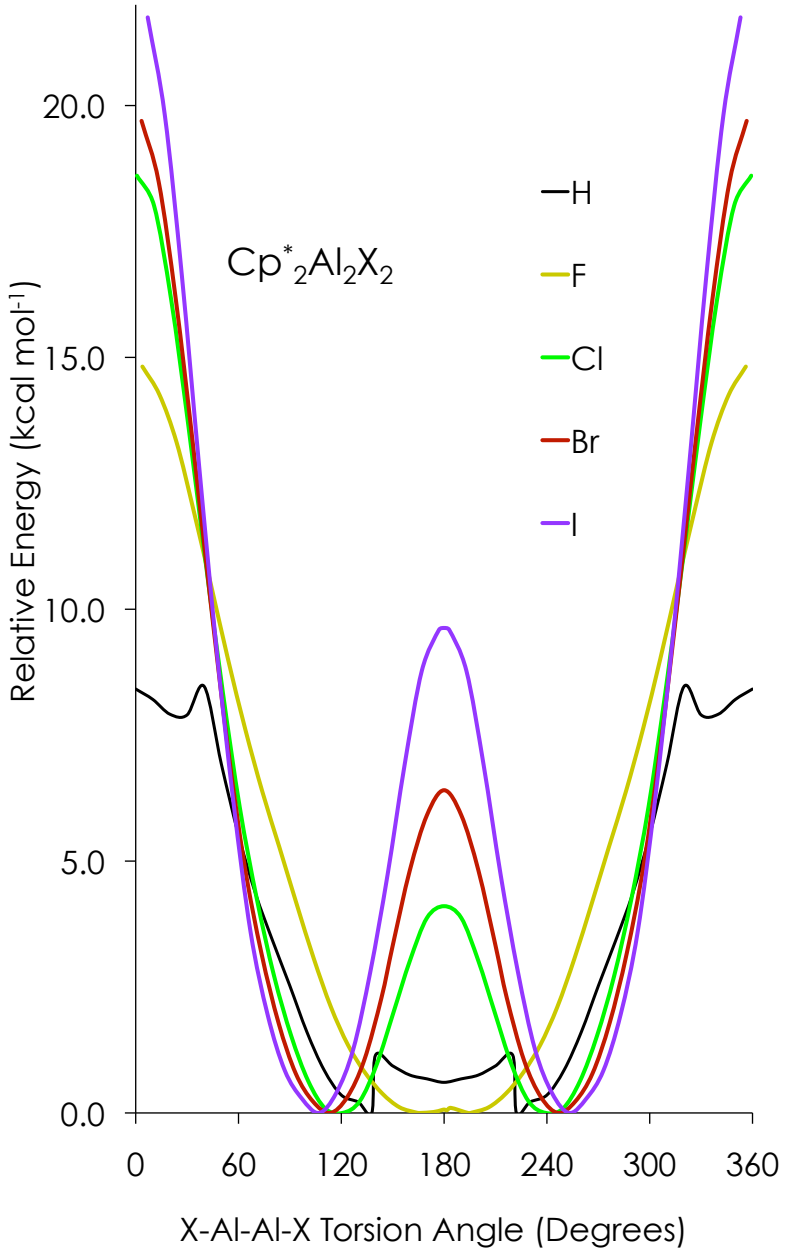

Figure 2.9: Torsional potential energy curves for $Cp^*_2Al_2X_2$ at the DZP SDB B3LYP level of theory.

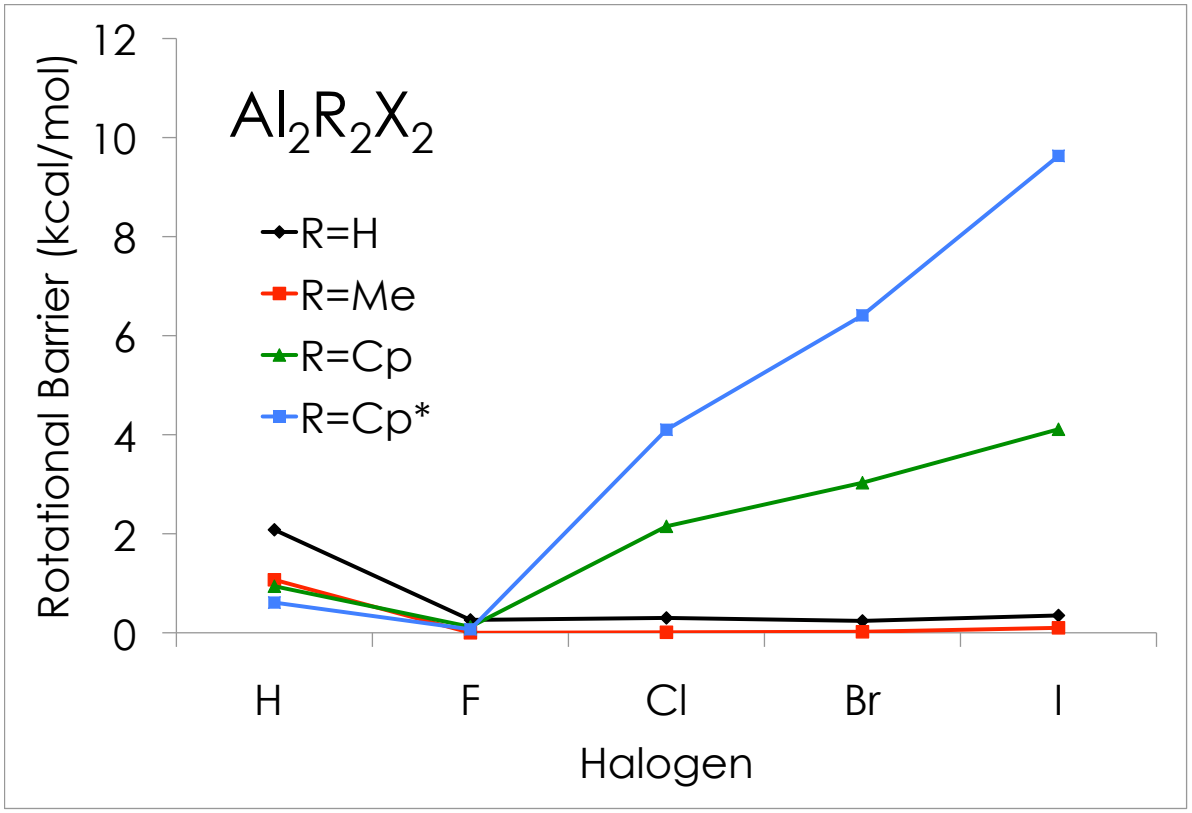

Figure 2.10: The Al−Al torsional barrier plotted against halogen substituent in aluminum dimetallocenes at the DZP SDB B3LYP level of theory.

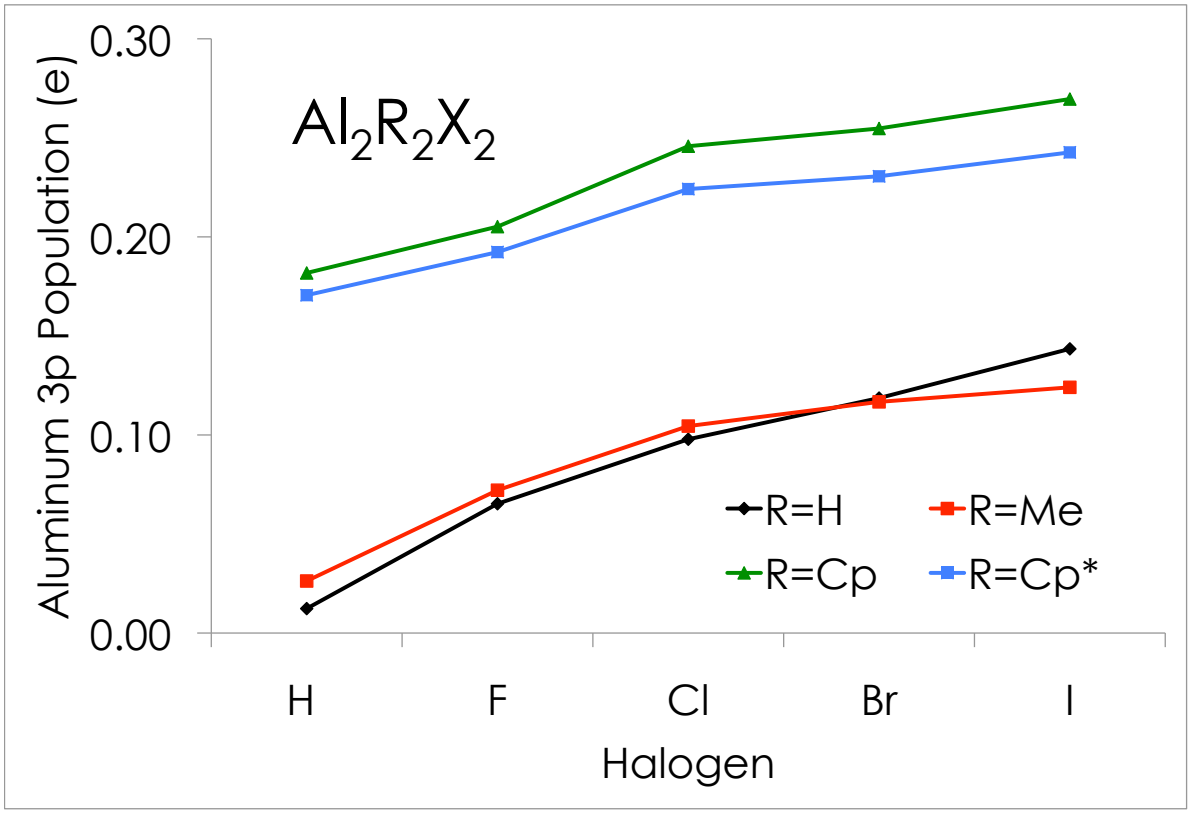

Figure 2.11: Aluminum lone-pair 3p NBO populations at the DZVP B3LYP level of theory.

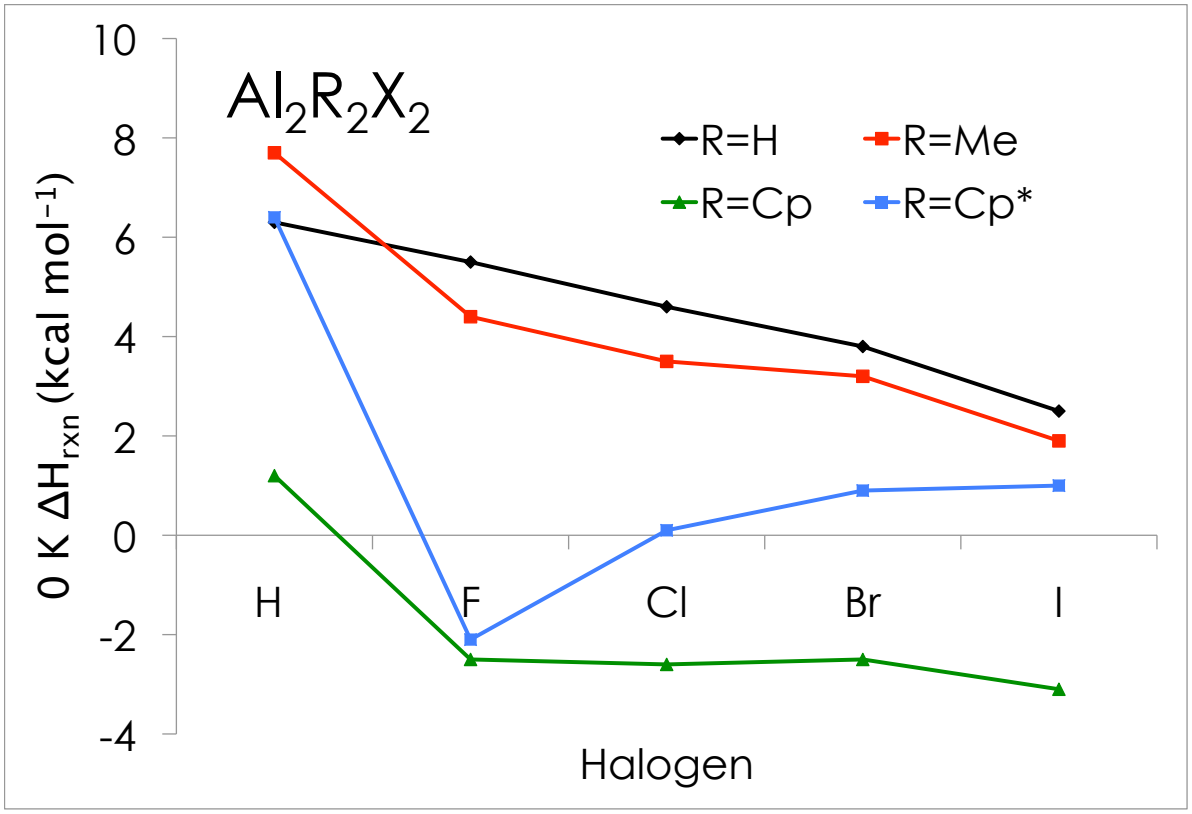

Figure 2.12: The dehydrogenation reaction enthalpy plotted against halogen substituent in aluminum dimetallocenes at the DZP SDB B3LYP level of theory.

CHAPTER 3

TOWARD DETECTION OF $AlCH_2$ IN THE INTERSTELLAR MEDIUM[1]

[1]Compaan, K., Dye, B., Yamaguchi, Y., and Schaefer, H. To be submitted to *Journal of the American Chemical Society.*

3.1 Abstract

Highly accurate geometries have been computed for the possible interstellar molecules, $AlCH_2$ and $AlCH_2^+$, at the CCSD(T) cc-pwCVQZ level of theory. In addition to providing information about the rich chemistry occurring in the interstellar medium, detection of $AlCH_2$ and $AlCH_2^+$ in the ISM may provide an indirect means of detecting interstellar methylene. The neutral contains a single Al–C bond; it requires 85 kcal mol^{-1} to dissociate $AlCH_2$ to ground state methylene plus aluminum atom. In the cation, the Al–C interaction is considerably weaker and may be described as a half bond. $AlCH_2^+$ lies 37 kcal mol^{-1} lower in energy than methylene and aluminum cation. Since both $AlCH_2$ and its cation are thermodynamically stable with respect to dissociation, they may be detectable in the interstellar medium. To aid in this effort, highly accurate spectroscopic data, including rotational constants, centrifugal distortion constants, harmonic vibrational frequencies, and anharmonic vibrational frequencies, has been computed.

3.2 Introduction

$AlCH_2$ is likely to exist in the interstellar medium (ISM) since methylene[87] and several aluminum-bearing species[81–86] have already been detected. Similar reasoning regarding the abundance of Al and CN in the ISM led to computational studies of AlNC[90,91]. The initial computational work fueled experimental characterization of the molecule[91–96], and identification of AlNC in the ISM[81,89,97]. Identifying and quantifying molecules in the ISM is a crucial part of understanding the complex chemistry that occurs in space as small nuclei fuse to form heavier elements in hot cores[88,89].

Species such as $AlCH_2$ are also important for understanding fundamental aluminum chemistry[98]. $AlCH_2$ does exist in the gas phase[103–105], based on mass spectrometry of electron-impact-ionized trimethylaluminum [$Al(CH_3)_3$]. Fragmentation patterns suggest that both $AlCH_2$ and $AlCH_2^+$ are present, but isomerization to other connectivities, such as HAlCH, is unlikely[103]. This is likely because there is no straightforward way to form HAlCH from fragmentation of trimethylaluminum.

Before its detection experimentally in 1990, $AlCH_2$ was the subject of extensive computational studies. Theoretical work in the 1980's was inspired by the increasing use of organoaluminum catalysts[127] and the discovery of trimethylaluminum–diethyl ether complex[98]. Further motivation came from a series of experiments and computations on the aluminum-acetylene complex[103,128]. The first computational study was performed in 1980[98]. DZP CISD energies were computed at DZ SCF geometries. The lowest-lying electronic state of $AlCH_2$ is connected to ground state triplet methylene and ground state aluminum atom. Aluminum prefers to retain an $3s^2 3p$ configuration and form single bonds, rather than disrupting its doubly occupied 3s orbital to form multiple bonds.

In order to understand the preference for single-bonds more fully, Cook and coworkers performed computations on $AlCH_2$, $HAlCH_2$, and their boron analogs[99]. Although the

computations were only carried out at the HF STO-3G level, they were able to qualitatively explain why B-CH_2 is doubly bonded while Al-CH_2 is singly bonded. The boron 2s and 2p orbitals are close in energy to the methylene orbitals, allowing for effective mixing. However, in aluminum the valence 3s and 3p orbitals are higher in energy than the methylene MO's, and thus they do not mix as effectively[99].

$AlCH_2$ was revisited in 1990 at a slightly higher level of theory[100]. Its geometry was optimized at the CISD level of theory with a TZ2P basis set. Their results are in qualitative agreement with previous work. After the synthesis of $AlCH_2$ experimentally in 1990, further computations were required to explain the observed lack of isomerization to HAlCH[101]. Using the same theoretical methods as the 1990 paper, they found that the HAlCH isomer lies about 44 kcal mol^{-1} above the $AlCH_2$ isomer. Finally, in 1991, isotropic hyperfine coupling constants were computed at the UMP2 6-311G** level of theory[102] using the published structure of $AlCH_2$[100,101]. This was done in an effort to unravel electronic spin resonance (ESR) spectra.

There have been no coupled cluster computations on $AlCH_2$, despite the large amount of attention it attracted in the past. In addition, there are no computational studies on $AlCH_2^+$ to our knowledge. With the vast computational resources available today, a high-accuracy study of these two possible interstellar molecules seemed in good order. Here we provide highly accurate geometries, rotational constants, harmonic and anharmonic frequencies, and dipole moments for $AlCH_2$ and $AlCH_2^+$. In addition, we have computed the heats of reaction for $AlCH_2$ formation from Al and methylene, and for $AlCH_2^+$ formation from methylene and aluminum cation. These reaction energies provide a measure of how stable $AlCH_2$ and $AlCH_2^+$ are to dissociation to their respective fragments.

3.3 Methods

The structures of $AlCH_2$ and $AlCH_2^+$ were optimized in their C_{2v} ground electronic states ($^2B_1$ and $^3A_1$ respectively) using coupled-cluster with single, double, (CCSD)[8–10] and perturbative triple excitations [CCSD(T)][11]. We used the cc-pwCVXZ (X=D, T, Q) series of correlation consistent basis sets[111,129,130]. Preliminary results indicated that core-correlation is important in this system Table 3.1. Due to poor convergence of the cc-pCVXZ basis sets for second-row atoms, we switched from the cc-pCVXZ series to the weighted core-valence cc-pwCVXZ sets.

Relative energies were extrapolated to the complete basis set (CBS) limit using the focal point approach prescribed by Allen[12–15]. The columns in a focal point table correspond to levels of theory; the first column contains the HF relative energy, the second contains the MP2 correction to the HF estimate (δMP2), and so forth. See equation below.

$$\Delta \mathrm{E}_{CCSD(T)} = \Delta \mathrm{E}_{HF} + \delta[\mathrm{MP2}] + \delta[\mathrm{CCSD}] + \delta[\mathrm{CCSD(T)}] \tag{3.1}$$

We used a two-point extrapolation scheme for the HF energy[16,17]:

$$E_X = E_{CBS/HF} + (X+1)be^{-9\sqrt{X}}\,. \tag{3.2}$$

In this equation, X is the cardinal number of the basis set (e.g. 2 corresponds to cc-pwCVDZ), $E_{CBS/HF}$ is the HF energy extrapolated to the CBS limit, and b is a fitting coefficient. We also used a two-point extrapolation for the correlation energy (E_{corr})[18].

$$E_X = E_{corr/CBS} + bX^{-3} \tag{3.3}$$

Here, X is the cardinal number of the basis set, $E_{corr/CBS}$ is the correlation energy, and b is a fitting coefficient. The best estimate of the relative energy appears in the bottom

right corner of the focal point table, and is the CCSD(T) result extrapolated to the CBS limit. Computations were carried out using the CFour 1.0[131] and Molpro 2010[118] program packages.

Natural bond orbital (NBO)[119–122] analysis based on the HF cc-pwCVDZ density matrix was carried out using the NBO 5.0 package in QChem 3.2[23].

3.4 Results and Discussion

3.4.1 Geometries and Spectroscopic Constants

The geometry of $AlCH_2$ was optimized in its $^2B_1$ electronic ground state at the CCSD(T) cc-pwCVQZ level of theory, using numerical derivatives and an ROHF reference wave function. It is shown in Figure 3.1. The geometry of $AlCH_2^+$ (Figure 3.2) was optimized in its $^3B_1$ electronic ground state at the CCSD(T) cc-pwCVQZ level of theory, using ROHF molecular orbitals and analytic derivatives. The geometric parameters are presented in Table 3.2, along with comparison to ground state $^3B_1$ CH_2 geometries at the CCSD(T) cc-pwCVQZ level of theory. Interestingly, the Al–C bond distance is 1.962Å in the neutral, but 1.909Å in the cation. This shortening is examined further in the NBO section (see below).

The harmonic frequencies of $AlCH_2$ and $AlCH_2^+$ were computed at the CCSD(T) cc-pwCVQZ level of theory, using analytic second derivatives. The results are presented in Table 3.3. A cubic force field was also computed, in order to determine anharmonic frequencies, vibrationally averaged rotational constants, and centrifugal distortion constants. These spectroscopic constants are presented in Table 3.4. It is crucial to correct the rotational constants for zero-point vibrational energies, since even small effects could move the rotational lines into a different spectral window. (Computations will finish soon. More discussion forthcoming on this point.)

Methylene is difficult to detect in the ISM because other interstellar species obscure its rotational transitions[87]. The methylene rotational constants are altered significantly by complexing with aluminum, so detection of $AlCH_2$ or $AlCH_2^+$ could be indirect means of quantifying interstellar methylene. Furthermore, although all three species addressed in Table 3.4 are asymmetric tops, both $AlCH_2$ and $AlCH_2^+$ are very close to being prolate symmetric tops. Their asymmetry parameters (κ) are very close to -1. The rotational spectra of $AlCH_2$ and $AlCH_2^+$ will thus be much cleaner than that of CH_2, and easier to assign.

3.4.2 Thermodynamics

We computed the thermodynamics of the following reaction:

$$CH_2 + Al \rightarrow AlCH_2 \ . \tag{3.4}$$

At the CCSD(T) cc-pwCVQZ level of theory, the ΔE_{rxn} is -84.8 kcal mol^{-1}. Extrapolation to the CBS CCSDT(Q) limit increases the exothermicity slightly, and yields a value of -86.0 kcal mol^{-1}. The relative energy has converged to within about 0.5 kcal mol^{-1} with respect to both basis set (rows) and level of theory (columns). Inclusion of CCSD(T) cc-pwCVQZ harmonic zero-point vibrational energy (ZPVE) yields the 0 K ΔH_{rxn}, which is -84.1 kcal mol^{-1} at the CBS CCSDT(Q) limit. These large negative reaction energies indicate that $AlCH_2$ is thermodynamically stable with respect to fragmentation. The ΔE can be interpreted as the Al–C bond energy; a bond energy of 85 kcal mol^{-1} is indicative of a single covalent bond. The formation of $AlCH_2$ from ground state Al atom and methylene should be a barrierless radical-radical reaction. Thus, the abundance of $AlCH_2$ is only dependent on the availability of the reactants and not temperature. This data suggests that $AlCH_2$

should be detectable in the ISM. Any methylene molecules which collide with Al atoms in the proper orientation will be trapped in a significant potential energy well as $AlCH_2$.

Next, we computed the thermodynamics of the corresponding cationic reaction:

$$CH_2 + Al^+ \rightarrow AlCH_2^+ \ . \tag{3.5}$$

The ΔE_{rxn} is -37.2 kcal mol^{-1} at the CCSD(T) cc-pwCVQZ level of theory. Inclusion of ZPVE decreases the magnitude of the reaction energy slightly, giving a value of ΔH_{rxn} equal to $-3...$ kcal mol^{-1}. (Focal point analysis forthcoming.) Although the Al–C bond is not as strong as in the neutral species, $AlCH_2^+$ is still significantly bound with respect to methylene and aluminum cation. This ion-radical reaction is barrierless, like the neutral reaction, meaning that $AlCH_2^+$ should also be observable in the ISM.

3.4.3 NBO Analysis

NBO analysis was performed using a HF cc-pVTZ density matrix, since the qualitative NBO results are not sensitive to correlation treatment[123].

In neutral $AlCH_2$, the natural charges indicate that the aluminum atom bears a significant positive charge in $AlCH_2$ (+0.73). The carbon has a -1.03 charge, and the hydrogens are slightly positive (+0.15). The unpaired electron is localized on the carbon atom, indicating that negative charge and spin density overlap spatially in $AlCH_2$. This is consistent with the bonding picture of $AlCH_2$, in which the 3p orbital of aluminum and the singly-occupied a_1 orbital from methylene overlap to form a single bond. The unpaired electron resides in the b_1 orbital of methylene, resulting in an overall $^2B_1$ wavefunction symmetry. Well over 99% of the electron density can be accounted for using a Lewis bonding scheme.

The Al–C bonding orbital is comprised of 90% methylene character and 10% aluminum 3p character. There is a nearly pure s-character lone pair on aluminum. The singly occupied

orbital on methylene has pure p character, but is only occupied by 0.95 electrons. About 0.05 electrons delocalize into an empty p orbital on aluminum, lending slight double bond character to the Al–C interaction. This delocalization from LP C $\rightarrow$ LP* Al is worth about 16 kcal mol^{-1} according to second-order perturbation analysis. The core orbitals and C–H bonds are exactly as expected.

The picture is considerably different in $AlCH_2^+$. The NBO algorithm describes the α-electron and β-electron density matrices separately. In the neutral, the descriptions qualitatively match up for all occupied orbitals. The dative bonding in the cation requires a more complicated bonding picture, and the α and β NBO's differ, even for formally doubly occupied orbitals. The $3s^2$ orbital on aluminum atom splits in this way. The α NBO is a lone-pair type orbital, with 85% s-character. It does not mix with any methylene MOs. However, the corresponding β NBO mixes significantly with methylene MOs, forming an Al–C bonding orbital. In addition to this one-electron bond, the methylene lone pairs delocalize into two empty 3p orbitals on aluminum cation, transferring a total of about 0.15 electrons to aluminum. Thus, in $AlCH_2^+$ there is slightly more than a "half bond" between aluminum and carbon. Compared to the neutral, the Al–C bond in the cation is shorter but weaker. This is because the 3p orbitals have a much larger spacial extent than the 3s orbitals. Since the 3p orbitals are all formally empty in $AlCH_2^+$, Al^+ can approach slightly closer to CH_2, even though the interaction is weaker.

3.5 Conclusions

Two possible interstellar molecules, $AlCH_2$ and $AlCH_2^+$, have been characterized using high-level *ab initio* methods. The thermodynamics of formation from aluminum atoms or cations and methylene indicate that these molecules are thermodynamically stable. Highly accurate spectroscopic constants have been provided, to aid in detection of these molecules in terrestrial laboratories and in the ISM.

3.6 Acknowledgement

Thanks to Dr. Andrew Simmonett, Dr. Justin Turney, and Dr. Wesley Allen for helpful discussions. Funding was provided by NSF Grant number CHE-1054286.

3.7 Tables

Property	ae cc-pCVTZ MP2	fc cc-pVTZ MP2	Δ
r(Al–C)	1.969	1.978	0.009
r(C–H)	1.088	1.090	0.001
θ(H–C–H)	110.1	110.1	< 0.1
Harmonic Frequencies	448.0	415.3	32.7
	482.8	547.4	64.5
	496.7	634.9	138.2
	1242.1	1394.2	152.1
	3118.1	3103.4	14.7
	3197.9	3190.6	7.3

Table 3.1: Comparison of frozen-core cc-pVTZ MP2 results to all-electron cc-pCVTZ MP2 results. Geometric paramters are in angstroms and degrees, harmonic frequencies are in wavenumbers. Note that the cc-pCVTZ basis set was designed to have the 1s orbitals on aluminum frozen.

Parameter	CH_2	$AlCH_2$	$AlCH_2^+$
r(Al–C)	n/a	1.962	1.909
r(C–H)	1.076	1.091	1.085
θ(H–C–H)	133.8	110.1	118.3

Table 3.2: Geometric parameters for $\tilde{X}\ ^3B_1$ methylene, $\tilde{X}\ ^2B_1$ $AlCH_2$ and $\tilde{X}\ ^3B_1$ $AlCH_2^+$ at the CCSD(T) cc-pwCVQZ level of theory. All distances are in angstroms, angles are in degrees.

Species	ω (cm^{-1})	ν (cm^{-1})	Symmetry	Description	I (km mol^{-1}
$AlCH_2$	3054.9		a_1	Symmetric C–H Stretch	22.4
	1386.4		a_1	CH_2 Scissor	2.7
	631.6		a_1	Al–C Stretch	95.2
	474.1		b_1	CH_2 Wag	3.9
	3135.2		b_2	Asymmetric C–H Stretch	12.4
	414.2		b_2	CH_2 Rock	3.0
$AlCH_2^+$	3113.5		a_1	Symmetric C–H Stretch	28.8
	1298.6		a_1	CH_2 Scissor	17.2
	647.9		a_1	Al–C Stretch	1.3
	705.7		b_1	CH_2 Wag	67.3
	3240.4		b_2	Asymmetric C–H Stretch	26.1
	575.4		b_2	CH_2 Rock	3.6

Table 3.3: Harmonic vibrational frequencies of $\tilde{X}\ ^2B_1$ $AlCH_2$ and $\tilde{X}\ ^1A_1$ $AlCH_2^+$ at the CCSD(T) cc-pwCVTZ level of theory. Anharmonic correction computed at the CCSD(T) cc-pwCVDZ level of theory. Descriptions and IR intensities (I) also provided.

	CH_2	$AlCH_2$	$AlCH_2^+$
A_e	54.820286	10.455239	9.644081
B_e	8.543536	0.426719	0.455177
C_e	7.391585	0.409986	0.434662
κ	−0.951	−0.997	−0.996
A_0			
B_0			
C_0			
Δ (MHz)			
μ	−0.238	0.323	−0.605

Table 3.4: Spectroscopic constants for $\tilde{X}\ ^3B_1$ methylene, $\tilde{X}\ ^2B_1$ $AlCH_2$ and $\tilde{X}\ ^1A_1$ $AlCH_2^+$ at the CCSD(T) cc-pwCVQZ level of theory. Rotational constants in cm^{-1}, CCSD dipole moments in debye.

	ΔE_{HF}	$+\delta$[MP2]	$+\delta$[CCSD]	$+\delta$[CCSD(T)]	$+\delta$[CCSDT]	NET
cc-pwCVDZ-DK	−52.42	−24.31	+2.10	−1.69	−0.07	-76.39
cc-pwCVTZ-DK	−54.83	−28.69	+2.70	−2.26	+0.03	[−83.06]
cc-pwCVQZ-DK	−54.95	−30.47	+2.97	−2.42	[+0.03]	[−84.83]
cc-pwCV5Z-DK	−54.96	−31.20	+3.21	−2.48	[+0.03]	[−85.40]
CBS LIMIT	[−54.96]	[−31.96]	[+3.46]	[−2.54]	[+0.03]	[−85.97]

Table 3.5: Focal point analysis of the reaction energy for $AlCH_2 \rightarrow CH_2 + Al$ in kcal mol^{-1}. Energies were computed at CCSD(T) cc-pwCVQZ geometries.

3.8 Figures

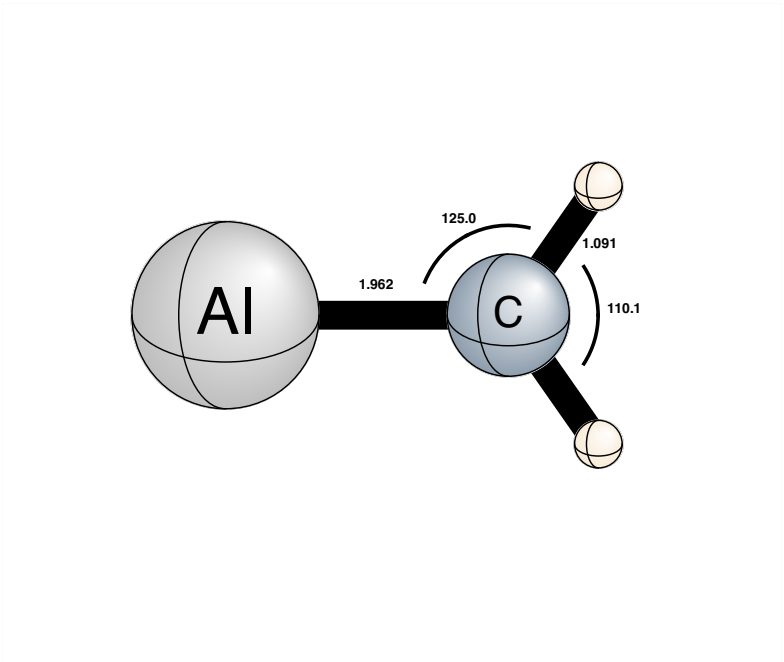

Figure 3.1: Structure of $AlCH_2$ at the CCSD(T) cc-pwCVQZ level of theory. Bond lengths are in angstroms, bond angles in degrees.

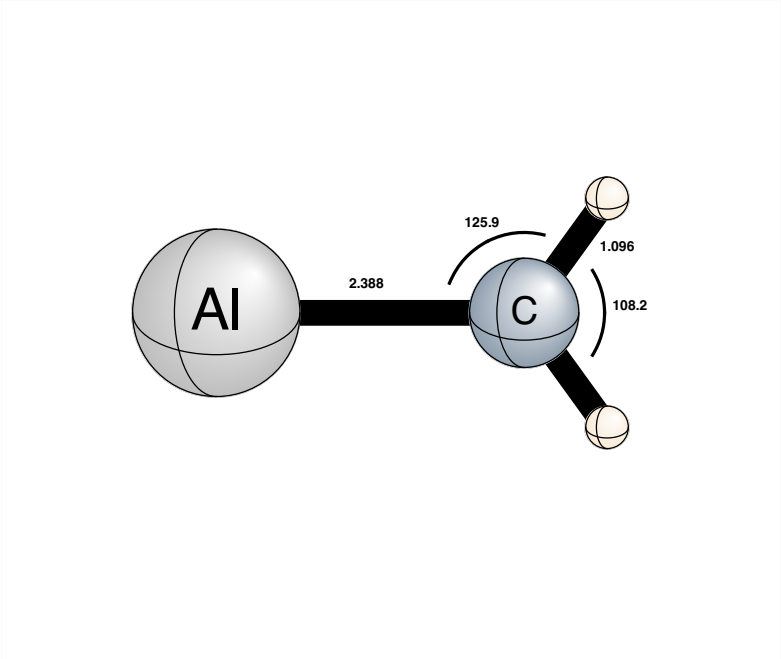

Figure 3.2: Structure of $AlCH_2^+$ at the CCSD(T) cc-pwCVQZ level of theory. Bond lengths are in angstroms, bond angles in degrees.

CHAPTER 4

CONCLUSIONS

Computational chemistry is a powerful tool for exploring new areas of chemistry. In this dissertation, its utility in investigating both large and small aluminum-containing systems has been amply demonstrated. In the first paper, ligand effects in the large molecule $Cp^*_2Al_2I_2$, which was only recently synthesized, were computed. Since DFT was a necessity for this project, various functionals were benchmarked against the experimental structure of $Cp^*_2Al_2I_2$ and against accurate *ab initio* results on model systems. Torsional potential energy curves were computed for a family of molecules relate to $Cp^*_2Al_2I_2$. I used NBO analysis to show the interplay between hyperconjugative and steric effects, which is dependent on both the size and electronic nature of the ligands. It is hoped that our computations on this new family of dialanes will inspire and guide future synthetic efforts.

Highly accurate coupled cluster methods were applied to $AlCH_2$ and its cation. This dissertation is the first computational work on $AlCH_2^+$. We found that both molecules are thermodynamically stable with respect to dissociation to CH_2+$Al^{(+)}$, and thus should be present in the ISM. This project highlights the role of coupled cluster methods; highly accurate geometries are required to determine useful spectroscopic constants. Lower level computations are simply insufficient, and provide no useful information to astrochemists seeking to identify new molecules in the ISM. Our results should be of great use to experimental groups, both in the fields of astrochemistry and fundamental organoaluminum studies.

Theory and experiment must work in tandem, to push the field of chemistry to new heights. In both of these projects, my computational work was based on previous experimental data, and should foster further experiments. In the case of $Cp^*_2Al_2I_2$, a novel structure published in Chemical Communications inspired a sweeping survey of dialane chemistry, and furthered our understanding of the intramolecular interactions which govern torsional potentials. In turn, we provided experimentalists with a systematic survey of new candidates for synthesis. The $AlCH_2$ project was motivated by the experimental detection of aluminum species and CH_2 in the ISM. The computations were specifically carried out to provide useful information to spectroscopists and astrochemists, in the expectation that the results will soon prove useful.

BIBLIOGRAPHY

[1] D. R. Lide, editor, *CRC Handbook of Chemistry and Physics*, CRC Press, Boca Raton, FL 33487, 88 edition, 2008.

[2] M. N. S. Rao, H. W. Roesky, and G. Anantharaman, *J. Organomet. Chem.* **646**, 4 (2002).

[3] C. Dohmeier, D. Loos, and H. Schnöckel, *Angew. Chem. Int. Ed. Engl.* **35**, 129 (1996).

[4] S. Nagendran and H. W. Roesky, *Organometallics* **27**, 457 (2008).

[5] E. Schrödinger, *Phys. Rev.* **28**, 1049 (1926).

[6] M. Born and R. Oppenheimer, *Ann. Phys.-Berlin* **389**, 457 (1927).

[7] F. Jensen, *Introduction to Computational Chemistry*, John Wiley and Sons, Ltd., 2 edition, 2007.

[8] J. Ĉížek, *J. Chem. Phys.* **45**, 4256 (1966).

[9] T. D. Crawford and H. F. Schaefer, *Rev. Comp. Chem.* **14**, 33 (2000).

[10] G. D. Purvis and R. J. Bartlett, *J. Chem. Phys.* **76**, 1910 (1982).

[11] K. Raghavachari, G. W. Trucks, J. A. Pople, and M. Head-Gordon, *Chem. Phys. Lett.* **157**, 479 (1989).

[12] A. G. Császar, W. D. Allen, and H. F. Schaefer, *J. Chem. Phys.* **108**, 9751 (1998).

[13] A. L. L. East and W. D. Allen, *J. Chem. Phys.* **99**, 4638 (1993).

[14] J. M. Gonzales, C. Pak, R. S. Cox, W. D. Allen, H. F. Schaefer, A. G. Csász, and G. Tarczay, *Chem. Eur. J.* **9**, 2173 (2003).

[15] R. A. King, W. D. Allen, and H. F. Schaefer, *J. Chem. Phys.* **112**, 5585 (2000).

[16] A. Karton and J. M. L. Martin, *Theor. Chem. Acc.* **115**, 330 (2006).

[17] W. Klopper and W. Kutzelnigg, *J. Mol. Struc.* **135**, 339 (1986).

[18] T. Helgaker, W. Klopper, H. Koch, and J. Noga, *J. Chem. Phys.* **106**, 9639 (1997).

[19] K. R. Compaan, J. J. Wilke, and H. F. Schaefer, *J. Am. Chem. Soc.* **133**, 13387 (2011).

[20] E. Runge and E. K. U. Gross, *Phys. Rev. Lett.* **52**, 997 (1984).

[21] A. D. Becke, *J. Chem. Phys.* **98**, 5648 (1993).

[22] C. Lee, W. Yang, and R. G. Parr, *Phys. Rev. B* **37**, 785 (1988).

[23] Y. Shao, L. Fusti-Molnar, Y. Jung, J. Kussmann, C. Ochsenfeld, S. T. Brown, A. T. B. Gilbert, L. V. Slipchenko, S. V. Levchenko, D. P. O'Neill, R. A. D. Jr., R. C. Lochan, T. Wang, G. J. O. Beran, N. A. Besley, J. M. Herbert, C. Y. Lin, T. V. Voorhis, S. H. Chien, A. Sodt, R. P. Steele, V. A. Rassolov, P. E. Maslen, P. P. Korambath, R. D. Adamson, B. Austin, J. Baker, E. F. C. Byrd, H. Dachsel, R. J. Doerksen, A. Dreuw, B. D. Dunietz, A. D. Dutoi, T. R. Furlani, S. R. Gwaltney, A. Heyden, S. Hirata, C.-P. Hsu, G. Kedziora, R. Z. Khalliulin, P. Klunzinger, A. M. Lee, M. S. Lee, W. Liang, I. Lotan, N. Nair, B. Peters, E. I. Proynov, P. A. Pieniazek, Y. M. Rhee, J. Ritchie, E. Rosta, C. D. Sherrill, A. C. Simmonett, J. E. Subotnik, H. L. W. III, W. Zhang, A. T. Bell, A. K. Chakraborty, D. M. Chipman, F. J. Keil, A. Warshel, W. J. Hehre, H. F. S. III, J. Kong, A. I. Krylov, P. M. W. Gill, and M. Head-Gordon, *Phys. Chem. Chem. Phys.* **8**, 3172 (2006).

[24] S. G. Minasian and J. Arnold, *Chem. Commun.* , 4043 (2008).

[25] Y. Xie, R. S. Grev, J. Gu, H. F. Schaefer, P. von Ragué Schleyer, J. Su, X.-W. Li, and G. H. Robinson, *J. Am. Chem. Soc.* **120**, 3773 (1998).

[26] Y. Wang, B. Quillian, P. Wei, C. S. Wannere, Y. Xie, R. B. King, H. F. Schaefer, P. von Ragué Schleyer, and G. H. Robinson, *J. Am. Chem. Soc.* **129**, 12412 (2007).

[27] B. Quillian, P. Wei, C. S. Wannere, P. von Ragué Schleyer, and G. H. Robinson, *J. Am. Chem. Soc.* **131**, 3168 (2009).

[28] R. J. Wehmschulte, K. Ruhlandt-Senge, M. M. Olmstead, H. Hope, B. E. Sturgeon, and P. P. Power, *Inorg. Chem.* **32**, 2983 (1993).

[29] N. Wiberg, K. Amelunxen, T. Blank, H. Nöth, and J. Knizek, *Organometallics* **17**, 5431 (1998).

[30] R. J. Wright, A. D. Phillips, and P. P. Power, *J. Am. Chem. Soc.* **125**, 10784 (2003).

[31] R. J. Wright, M. Brynda, and P. P. Power, *Angew. Chem. Int. Ed.* **45**, 5953 (2006).

[32] P. Henke, T. Pankewitz, W. Klopper, F. Breher, and H. Schnöckel, *Angew. Chem. Int. Ed.* **48**, 8141 (2009).

[33] M. Schormann, K. S. Klimek, H. Hatop, S. P. Varkey, H. W. Roesky, C. Lehmann, C. Röpken, R. Herbst-Irmer, and M. Noltemeyer, *J. Solid State Chem.* **624**, 513 (2001).

[34] C. Üffing, A. Ecker, R. Köppe, and H. Schnöckel, *Organometallics* **17**, 2373 (1998).

[35] C. K. F. von Hänisch, C. Üffing, M. A. Junker, A. Ecker, B. O. Kneisel, and H. Schnöckel, *Angew. Chem. Int. Ed. Engl.* **35**, 2875 (1996).

[36] S. Schulz, T. Schoop, H. W. Roesky, L. Häming, A. Steiner, and R. Herbst-Irmer, *Angew. Chem. Int. Ed. Engl.* **34**, 919 (1995).

[37] C. Dohmeier, H. Krautscheid, and H. Schnöckel, *Angew. Chem. Int. Ed. Engl.* **33**, 2482 (1994).

[38] J. D. Gorden, A. Voigt, C. L. B. Macdonald, J. D. Silverman, and A. H. Cowley, *J. Am. Chem. Soc.* **122**, 950 (2000).

[39] A. Purath, C. Dohmeier, A. Ecker, R. Köppe, H. Krautscheid, H. Schnöckel, R. Ahlrichs, C. Stoermer, J. Friedrich, and P. Jutzi, *J. Am. Chem. Soc.* **122**, 6955 (2000).

[40] A. Y. Timoshkin, *Coord. Chem. Rev.* **249**, 2094 (2005).

[41] S. Schulz, L. Häming, R. Herbst-Irmer, H. W. Roesky, and G. M. Sheldrick, *Angew. Chem. Int. Ed. Engl.* **33**, 969 (1994).

[42] W. Hiller, K.-W. Klinkhammer, W. Uhl, and J. Wagner, *Angew. Chem. Int. Ed. Engl.* **30**, 179 (1991).

[43] C. Dohmeier, M. Mocker, H. Schnöckel, A. Lötz, U. Schneider, and R. Ahlrichs, *Angew. Chem. Int. Ed. Engl.* **32**, 1428 (1993).

[44] A. Ecker, E. Weckert, and H. Schnöckel, *Nature* **387**, 379 (1997).

[45] C. Üffing, E. Baum, R. Köppe, and H. Schnöckel, *Angew. Chem. Int. Ed.* **37**, 2397 (1998).

[46] A. Purath, R. Köppe, and H. Schnöckel, *Angew. Chem. Int. Ed.* **38**, 2926 (1999).

[47] W. Uhl and F. Breher, *Angew. Chem. Int. Ed.* **38**, 1477 (1999).

[48] W. Uhl, B. Breher, A. Mbonimana, J. Gauss, D. Haase, A. Lützen, and W. Saak, *Eur. J. Inorg. Chem.* **2001**, 3059 (2001).

[49] J. Vollet, J. R. Hartig, and H. Schnöckel, *Angew. Chem. Int. Ed.* **43**, 3186 (2004).

[50] J. Vollet, R. Burgert, and H. Schnöckel, *Angew. Chem. Int. Ed.* **44**, 6956 (2005).

[51] W. Uhl, *Z. Naturforsch.* **43b**, 1113 (1988).

[52] J. W. Turley and H. W. Rinn, *Inorg. Chem.* **8**, 18 (1969).

[53] M. Huber and H. Schnöckel, *Inorg. Chim. Acta* **361**, 457 (2008).

[54] W. Uhl, A. Vester, W. Kaim, and J. Poppe, *J. Organomet. Chem.* **454**, 9 (1993).

[55] C. Pluta, K.-R. Pörschke, C. Krüger, and K. Hildenbrand, *Angew. Chem. Int. Ed. Engl.* **32**, 388 (1993).

[56] Y. Wang and G. H. Robinson, *Organometallics* **26**, 2 (2007).

[57] A. Ecker, E. Baum, M. A. Friesen, M. A. Junker, C. Üffing, and H. Schnöckel, *Z. anorg. allg. Chem.* **624**, 513 (1998).

[58] C. Klemp, C. Üffing, E. Baum, and H. Schnöckel, *Z. anorg. allg. Chem.* **626**, 1787 (2000).

[59] M. Mocker, C. Robl, and H. Schnöckel, *Angew. Chem. Int. Ed. Engl.* **33**, 862 (1994).

[60] C. Dohmeier, C. Robl, M. Tacke, and H. Schnöckel, *Angew. Chem. Int. Ed. Engl.* **30**, 564 (1991).

[61] H. Sitzmann, M. F. Lappert, C. Dohmeier, C. Üffing, and H. Schnöckel, *J. Organomet. Chem.* **561**, 203 (1998).

[62] U. Schneider, R. Ahlrichs, H. Horn, and A. Schäfer, *Angew. Chem. Int. Ed. Engl.* **31**, 353 (1992).

[63] A. Purath, C. Dohmeier, A. Ecker, and H. Schnöckel, *Organometallics* **17**, 1894 (1998).

[64] C. Schnitter, H. W. Roesky, C. Röpken, R. Herbst-Irmer, H.-G. Schmidt, and M. Noltemeyer, *Angew. Chem. Int. Ed.* **37**, 1952 (1998).

[65] A. Purath and H. Schnöckel, *J. Organomet. Chem.* **579**, 373 (1999).

[66] M. Scheifer, N. D. Reddy, H. W. Roesky, and D. Vidovic, *Organometallics* **22**, 3637 (2003).

[67] X. Li, A. Brubisic, S. T. Stokes, J. Cordes, G. F. Ganteför, K. H. Bowen, B. Kiran, M. Willis, P. Jena, R. Burgert, and H. Schnöckel, *Science* **315**, 356 (2007).

[68] P. Henke, M. Huber, J. Steiner, K. Bowen, B. Eichhorn, and H. Schnöckel, *J. Am. Chem. Soc.* **131**, 5698 (2009).

[69] W. Uhl, *Naturwissenschaften* **91**, 305 (2004).

[70] M. Huber, P. Henke, and H. Schnöckel, *Chem. Eur. J.* **15**, 12180 (2009).

[71] R. Ahlrichs, M. Ehrig, and H. Horn, *Chem. Phys. Lett.* **183**, 227 (1991).

[72] J. Gauss, U. Schneider, R. Ahlrichs, C. Dohmeier, and H. Schnöckel, *J. Am. Chem. Soc.* **115**, 2402 (1993).

[73] T. Pankewitz, W. Klopper, P. Henke, and H. Schnöckel, *Eur. J. Inorg. Chem.* , 4879 (2008).

[74] K. Lammertsma and J. Leszczyǹski, *J. Phys. Chem.* **94**, 2806 (1990).

[75] L. Andrews and X. Wang, *Science* **299**, 2049 (2003).

[76] X. Wang, L. Andrews, S. Tam, M. E. DeRose, and M. E. Fajardo, *J. Am. Chem. Soc.* **125**, 9218 (2003).

[77] C. Liang, R. D. Davy, and H. F. Schaefer, *Chem. Phys. Lett.* **159**, 393 (1989).

[78] B. J. Duke, C. Liang, and H. F. Schaefer, *J. Am. Chem. Soc.* **113**, 2884 (1991).

[79] N. C. Baird, *Can. J. Chem.* **63**, 71 (1985).

[80] A. Szabó, A. Kovács, and G. Frenking, *Z. anorg. allg. Chem.* **631**, 1803 (2005).

[81] L. M. Ziurys, C. Savage, J. L. Highberger, A. J. Apponi, M. Guélin, and J. Cernicharo, *Astrophys. J.* **564**, L45 (2002).

[82] J. L. Highberger, C. Savage, J. H. Bieging, and L. M. Ziurys, *Astrophys. J.* **562**, 790 (2001).

[83] J. Cernicharo and M. Guélin, *Astron. Astrophys.* **183**, L10 (1987).

[84] E. D. Tenenbaum and L. M. Ziurys, *Astrophys. J. Lett.* **712**, L93 (2010).

[85] E. D. Tenenbaum and L. M. Ziurys, *Astrophys. J. Lett.* **694**, L59 (2009).

[86] L. M. Ziurys, A. J. Apponi, and T. G. Phillips, *Astrophys. J.* **433**, 729 (1994).

[87] J. M. Hollis, P. R. Jewell, and F. J. Lovas, *Astrophys. J.* **438**, 259 (1995).

[88] W. Klemperer, *P. Natl. Acad. Sci. USA* **103**, 12232 (2006).

[89] L. M. Ziurys, *P. Natl. Acad. Sci. USA* **103**, 12274 (2006).

[90] B. Ma, Y. Yamaguchi, and H. F. Schaefer, *Mol. Phys.* **86**, 1331 (1995).

[91] D. Stöckigt, M. C. Holthausen, W. Koch, and H. Schwarz, *J. Phys. Chem.* **99**, 5950 (1995).

[92] D. V. Lanzisera and L. Andrews, *J. Phys. Chem. A* **101**, 9660 (1997).

[93] K. A. Walker and M. C. L. Gerry, *Chem. Phys. Lett.* **278**, 9 (1997).

[94] J. S. Robinson, A. J. Apponi, and L. M. Ziurys, *Chem. Phys. Lett.* **278**, 1 (1997).

[95] I. Gerasimov, X. Yang, and P. J. Dagdigian, *J. Chem. Phys.* **110**, 220 (1999).

[96] K. A. Walker, C. J. Evans, S.-H. K. Suh, M. C. L. Gerry, and J. K. G. Watson, *J. Mol. Spectrosc.* **209**, 179 (2001).

[97] S. Petrie and D. K. Bohme, *Top. Curr. Chem.* **225**, 37 (2003).

[98] D. J. Fox, D. Ray, P. C. Rubesin, and H. F. Schaefer, *J. Chem. Phys.* **73**, 3246 (1980).

[99] C. M. Cook and L. C. Allen, *Organometallics* **1**, 246 (1982).

[100] S. Q. Jin, Y. Xie, and H. F. Schaefer, *Chem. Phys. Lett.* **170**, 301 (1990).

[101] S. Q. Jin, Y. Xie, and H. F. Schaefer, *J. Chem. Phys.* **95**, 1834 (1991).

[102] C. J. Cramer, *J. Mol. Struc-Theochem* **235**, 243 (1991).

[103] R. Srinivas, D. Sülzle, and H. Schwarz, *J. Am. Chem. Soc.* **112**, 8334 (1990).

[104] D. V. Zagorevskii and J. L. Holmes, *Mass Spectrom. Rev.* **18**, 87 (1999).

[105] D. V. Zagorevskii, *Coord. Chem. Rev.* **225**, 5 (2002).

[106] Y. Osamura, H. F. Schaefer, S. K. Gray, and W. H. Miller, *J. Am. Chem. Soc.* **103**, 1904 (1981).

[107] S. Joseph and A. J. C. Varandas, *J. Phys. Chem. A* **114**, 13277 (2010).

[108] J. D. Dill, P. von Ragué Schleyer, and J. A. Pople, *J. Am. Chem. Soc.* **97**, 3402 (1975).

[109] T. H. Dunning Jr., *J. Chem. Phys.* **90**, 1007 (1989).

[110] D. E. Woon and T. H. Dunning Jr., *J. Chem. Phys.* **98**, 1358 (1993).

[111] T. H. Dunning Jr., *J. Chem. Phys.* **90**, 1007 (1989).

[112] D. E. Woon and T. H. Dunning Jr., *J. Chem. Phys.* **98**, 1358 (1993).

[113] N. J. DeYonker, K. A. Peterson, and A. K. Wilson, *J. Phys. Chem. A* **111**, 11383 (2007).

[114] F. Weinhold, *Encyclopedia of Computational Chemistry*, volume 3, pp. 1792–1811, John Wiley and Sons, Ltd., 1998.

[115] N. Godbout, D. R. Salahub, J. Andzelm, and E. Wimmer, *Can. J. Chem.* **70**, 560 (1992).

[116] T. H. Dunning Jr. and P. J. Hay, *Methods of Electronic Structure Theory*, volume 2, pp. 1–27, Plenum Press, 1977.

[117] A. Bergner, M. Dolg, W. Küchle, H. Stoll, and H. Preuss, *Mol. Phys.* **80**, 1431 (1993).

[118] H.-J. Werner, P. J. Knowles, G. Knizia, F. R. Manby, M. Schütz, P. Celani, T. Korona, R. Lindh, A. Mitrushenkov, G. Rauhut, K. R. Shamasundar, T. B. Adler, R. D. Amos, A. Bernhardsson, A. Berning, D. L. Cooper, M. J. O. Deegan, A. J. Dobbyn, F. Eckert, E. Goll, C. Hampel, A. Hesselmann, G. Hetzer, T. Hrenar, G. Jansen, C. Köppl, Y. Liu, A. W. Lloyd, R. A. Mata, A. J. May, S. J. McNicholas, W. Meyer, M. E. Mura, A. Nicklass, D. P. O'Neill, P. Palmieri, K. Pflüger, R. Pitzer, M. Reiher, T. Shiozaki, H. Stoll, A. J. Stone, R. Tarroni, T. Thorsteinsson, M. Wang, and A. Wolf, MOLPRO, version 2010.1, a package of ab initio programs, 2010.

[119] A. E. Reed, F. Weinhold, L. A. Curtiss, and D. J. Pochatko, *J. Chem. Phys.* **84**, 5687 (1986).

[120] A. E. Reed and F. Weinhold, *J. Chem. Phys.h* **78**, 4066 (1983).

[121] J. P. Foster and F. Weinhold, *J. Am. Chem. Soc.* **102**, 7211 (1980).

[122] A. E. Reed, R. B. Weinstock, and F. Weinhold, *J. Chem. Phys.* **83**, 735 (1985).

[123] F. Weinhold and C. Landis, *Valency and Bonding A Natural Bond Orbital Donor-Acceptor Perspective*, Cambridge University Press, Cambridge, UK, first edition, 2005.

[124] R. S. Mulliken, *J. Phys. Chem.* **56**, 801 (1952).

[125] R. S. Mulliken, *J. Am. Chem. Soc.* **74**, 811 (1952).

[126] J. Urban, P. R. Schreiner, G. Vacek, P. von Ragué Schleyer, J. Q. Huang, and J. Leszczyǹski, *Chem. Phys. Lett.* **264**, 441 (1997).

[127] T. Mole and E. A. Jeffery, *Organoaluminum Compounds*, Elsevier Science Ltd., Amsterdam, 1972.

[128] Y. Xie, B. F. Yates, and H. F. Schaefer, *J. Am. Chem. Soc.* **112**, 517 (1990).

[129] W. A. de Jong, R. J. Harrison, and D. A. Dixon, *J. Chem. Phys.* **114**, 48 (2001).

[130] K. A. Peterson and J. Thom H Dunning, *J. Chem. Phys.* **117**, 10548 (2002).

[131] Stanton, J. F.; Gau, J.;Harding M. E.; Szalay, P. G.; with contributions from Auer, A. A.;Bartlett, R. J.; Benedikt, U.; Berger, C.; Bernholdt, D. E.; Bomble, Y. J.; Cheng, L.; Christiansen, O.; Heckert, M.; Heun, O.; Huber, C.; Jagau, T.-C.; Jonsson, D.; Jusélius, J.; Klein, K.; Lauderdale, W. J.; Matthews, D. A.; Metzroth, T.; O'Neill, D. P.; Price, D. R.; Prochnow, E.; Ruud, K.; Schiffmann, F.; Schwalbach, W.; Stopkowicz, S.; Tajti, A.; Vázquez, J.; Wang, F.; Watts, J. D.; and the integral packages: Molecule (Almlöf, J.; Taylor, P. R.), Props (Taylor, P. R.), and Abacus (Helgaker, T.; Jensen, H. J. Aa.; Jørgensen, P.; Olsen, J.;). Current version see http://www.cfour.de.